



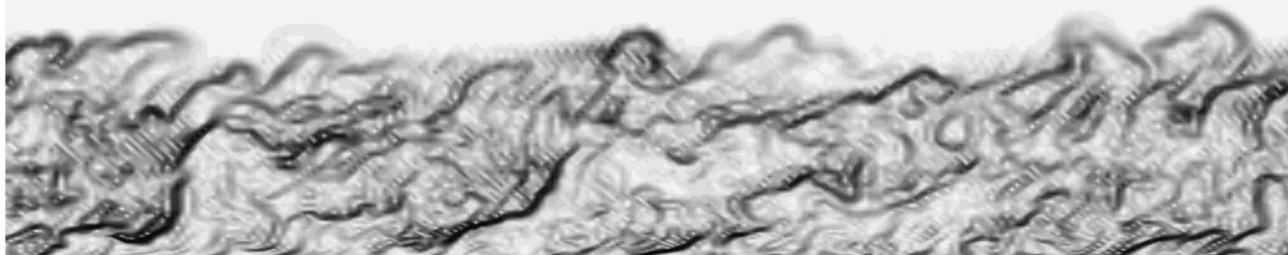
Investigation of Numerical Schemes for Direct Numerical Simulations of Supersonic Turbulent Boundary Layers

Christopher I. Morris

NASA Marshall Space Flight Center

Aerosciences Branch/EV33

January 9, 2015

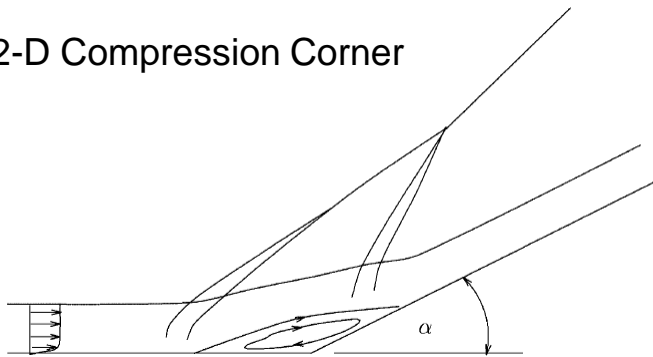




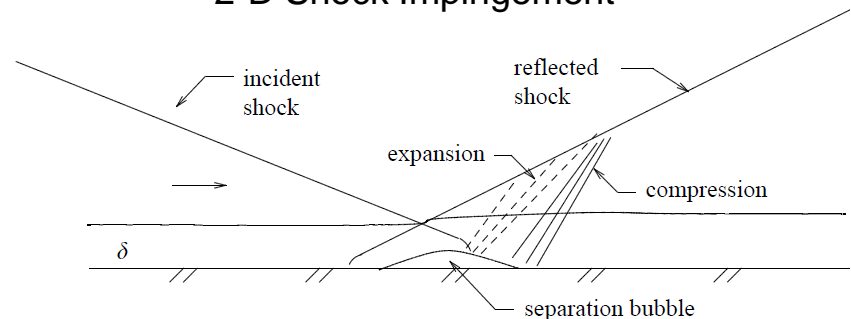
Objectives

- ◆ Determine the suitability of various inviscid flux schemes for DNS/LES of supersonic turbulent boundary layers - foundational for more complex turbulent flows in aerospace applications:
 - Shock-turbulent boundary layer interactions
 - Supersonic film cooling

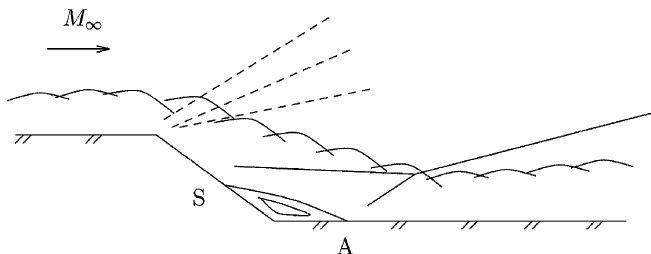
2-D Compression Corner



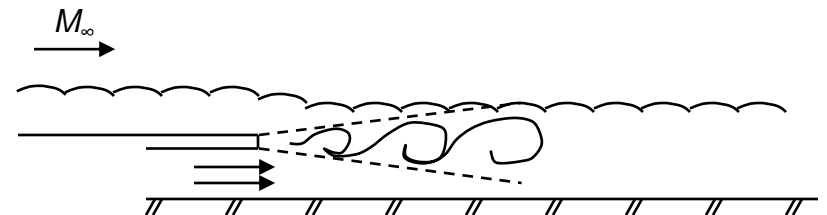
2-D Shock Impingement



2-D Expansion-Compression Corner



2-D Supersonic Film Cooling





Approach

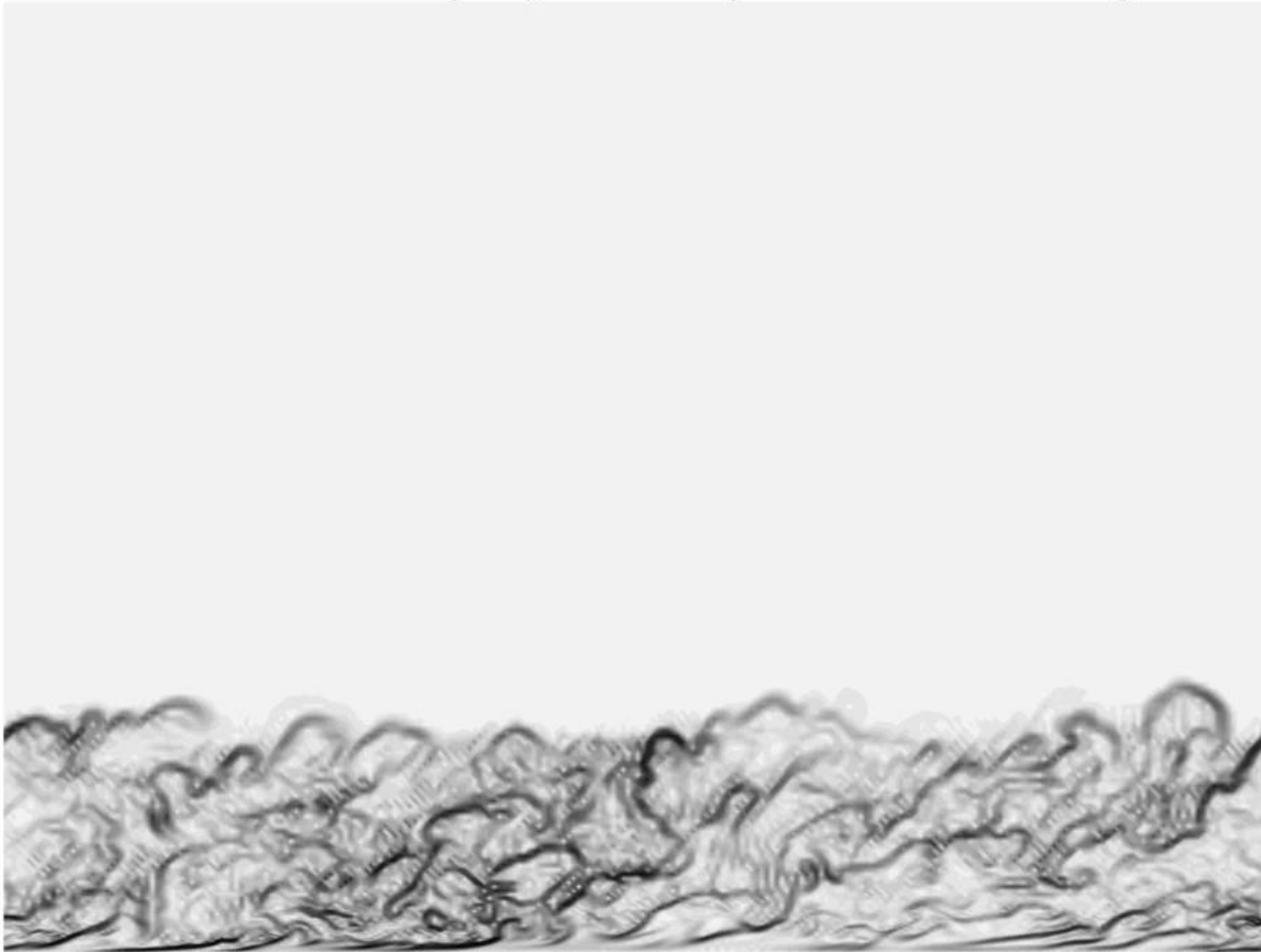
- ◆ **A number of approaches for DNS or LES of supersonic turbulent boundary layers have been used over the past two decades**
 - Fully spatially evolving simulations
 - Forced transition from laminar inflow BC
 - Quasi-turbulent inflow BC
 - Recycling of inflow BC from point further downstream
 - Extended temporally-developing simulations
 - Temporally-developing simulations

- ◆ **Temporally-developing approach used here**
 - Inexpensive: relatively small domain can be used
 - Allows spatial averaging and periodic boundary conditions in both streamwise (x) and spanwise (z) directions
 - Significant disadvantage is that the flow field is never truly statistically stationary – rather, the boundary layer slowly grows with time. However, Martin (2004, 2007) and Xu and Martin (2004) have shown that if a relatively short time window is chosen, good results can be obtained.



Temporally-Developing Turbulent Boundary Layer at Mach 2.889, $Re = 1.93 \times 10^6 \text{ m}^{-1}$

Turbulent Boundary Layer Flow - Synthetic Schlieren Image



Normalized Time: 11.50

- ◆ t^* is a normalized timescale $t U_\infty / 9.6L$ (domain flowthrough timescale)



Scope

- ◆ **Emphasis in this paper is on studying the basic resolving characteristics of spatial discretizations and inviscid flux schemes for this compressible flow problem, not on LES sub-grid scale (SGS) models**
- ◆ **Grid resolutions considered here are from DNS levels to fine-grid LES levels**
- ◆ **Adiabatic wall BC selected as this case is well-understood and Morkovin's hypothesis holds at Mach 5 and below**
- ◆ **Viscous discretization is 2nd-order accurate only (limited tests with higher-order accuracy do not appear to change results appreciably)**
- ◆ **Time advancement is 4-stage Runge-Kutta, limited by stability restrictions to time steps significantly smaller than those needed to resolve turbulence**



Governing Equations of Fluid Mechanics

Navier-Stokes Equations in Terms of Conservative Variables:

$$\frac{d\mathbf{U}}{dt} + \frac{d(\mathbf{F}_i - \mathbf{F}_v)}{dx} + \frac{d(\mathbf{G}_i - \mathbf{G}_v)}{dy} + \frac{d(\mathbf{H}_i - \mathbf{H}_v)}{dz} = \mathbf{W}$$

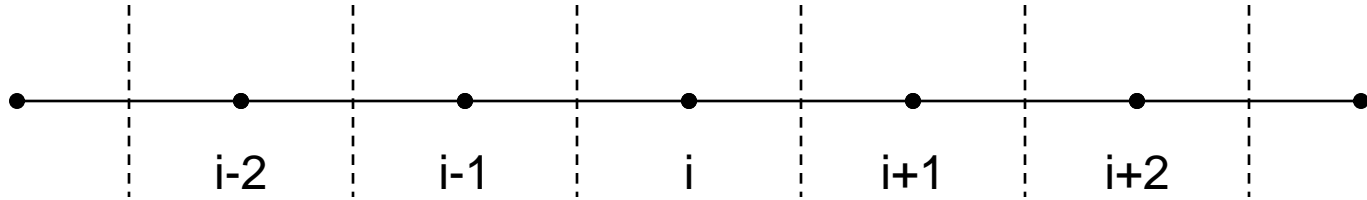
$$\mathbf{U} = \begin{Bmatrix} \rho \\ \rho u \\ \rho v \\ \rho w \\ \rho E_{\text{tot}} \end{Bmatrix} \quad \mathbf{F}_i = \begin{Bmatrix} \rho u \\ \rho u^2 + P \\ \rho uv \\ \rho uw \\ \rho u H_{\text{tot}} \end{Bmatrix} \quad \mathbf{F}_v = \begin{Bmatrix} 0 \\ T_{xx} \\ T_{xy} \\ T_{xz} \\ uT_{xx} + vT_{xy} + wT_{xz} - q_x \end{Bmatrix} \quad \text{Etc.}$$

Conservative Differencing Forms the Flux at a Half-Point:

$$\frac{d\mathbf{U}}{dt} + \frac{d\mathbf{F}(\mathbf{U})}{dx} = 0 \quad \Rightarrow \quad \frac{d\mathbf{U}}{dt} = -\frac{d\mathbf{F}(\mathbf{U})}{dx} \quad \Rightarrow \quad \Delta\mathbf{U}_i = -(\Delta t/\Delta x)(\mathbf{F}_{i+1/2} - \mathbf{F}_{i-1/2})$$



Skew-Symmetric Central Difference Schemes



$$\text{SSCD-2 } \mathbf{F}_{i+\frac{1}{2}} = \mathbf{F}_{\text{avg}}(i, i+1)$$

$$\text{SSCD-4 } \mathbf{F}_{i+\frac{1}{2}} = (4/3)\mathbf{F}_{\text{avg}}(i, i+1) - (1/6)[\mathbf{F}_{\text{avg}}(i-1, i+1) + \mathbf{F}_{\text{avg}}(i, i+2)]$$

$$\text{SSCD-6 } \mathbf{F}_{i+\frac{1}{2}} = (3/2)\mathbf{F}_{\text{avg}}(i, i+1) - (3/10)[\mathbf{F}_{\text{avg}}(i-1, i+1) + \mathbf{F}_{\text{avg}}(i, i+2)] \\ + (1/30)[\mathbf{F}_{\text{avg}}(i-2, i+1) + \mathbf{F}_{\text{avg}}(i-1, i+2) + \mathbf{F}_{\text{avg}}(i, i+3)]$$

$$\text{SSCD-8 } \mathbf{F}_{i+\frac{1}{2}} = (16/10)\mathbf{F}_{\text{avg}}(i, i+1) - (4/10)[\mathbf{F}_{\text{avg}}(i-1, i+1) + \mathbf{F}_{\text{avg}}(i, i+2)] \\ + (8/105)[\mathbf{F}_{\text{avg}}(i-2, i+1) + \mathbf{F}_{\text{avg}}(i-1, i+2) + \mathbf{F}_{\text{avg}}(i, i+3)] \\ - (1/140)[\mathbf{F}_{\text{avg}}(i-3, i+1) + \mathbf{F}_{\text{avg}}(i-2, i+2) + \mathbf{F}_{\text{avg}}(i-1, i+3) + \mathbf{F}_{\text{avg}}(i, i+4)]$$

$$\mathbf{F}_{\text{avg}}(i_1, i_2) = \rho_{\text{avg}} u_{\text{avg}} \mathbf{V}_{\text{avg}} + \mathbf{P}_{\text{avg}}$$

where $\mathbf{V}_{\text{avg}} = [1, u_{\text{avg}}, v_{\text{avg}}, w_{\text{avg}}, \mathbf{e}_{\text{avg}} + \frac{1}{2}(u_{\text{avg}}^2 + v_{\text{avg}}^2 + w_{\text{avg}}^2) + p_{\text{avg}}/\rho_{\text{avg}}]$
 and $\mathbf{P}_{\text{avg}} = [0, P_{\text{avg}}, 0, 0, 0]$

For any variable ϕ , $\phi_{\text{avg}} = \frac{1}{2}(\phi_{i_1} + \phi_{i_2})$. This \mathbf{F}_{avg} is very similar to the skew-symmetric scheme of Kennedy and Gruber (2008) (Also see Pirozzoli (2010)). Note if $\mathbf{F}_{\text{avg}} = (\mathbf{F}_{i_1} + \mathbf{F}_{i_2})$, then standard divergence form central differencing formulas result.



Filtered Central Difference Scheme

Eighth-Order Divergence Form Central Difference Scheme

$$\text{DCD-8} \quad \mathbf{F}_{i+\frac{1}{2}} = [-3\mathbf{F}_{i-3} + 29\mathbf{F}_{i-2} - 139\mathbf{F}_{i-1} + 533\mathbf{F}_i + 533\mathbf{F}_{i+1} - 139\mathbf{F}_{i+2} + 29\mathbf{F}_{i+3} - 3\mathbf{F}_{i+4}]/840$$

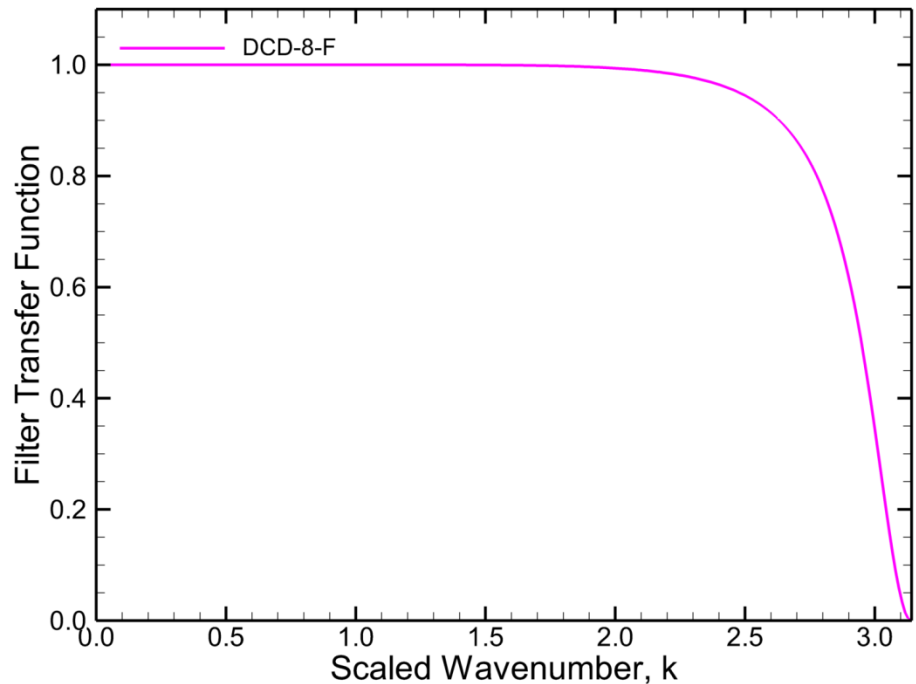
Combined with Compact Filtering Algorithm (Visbal and Gaitonde, 1999) at interior points, and High Order Boundary Filtering Algorithm (Gaitonde and Visbal, 2000) at the lower and upper domain boundaries.

The filter completely filters wavelengths at the spatial Nyquist frequency $k = \pi$ (2 p.p.w.)

The filter transfer function is > 0.999 at $k = \pi/2$ (4 p.p.w.), and is > 0.99 at $k = 2\pi/3$ (3 p.p.w.)

Filter is applied after one full Runge-Kutta timestep

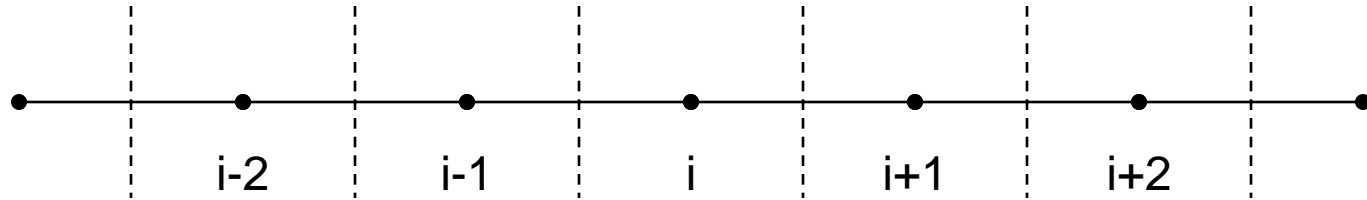
Filter Transfer Function at Interior Points



Combination of DCD-8 with filtering algorithm is referred to DCD-8-F in this work



Upwind-Biased Roe Schemes



Roe Flux using “left” and “right” interpolations for the half-node

$$\mathbf{F}_{i+1/2} = \frac{1}{2}(\mathbf{F}_{i+1/2,L} + \mathbf{F}_{i+1/2,R}) - \frac{1}{2}|\mathbf{A}_{\text{roe}}|(\mathbf{U}_{i+1/2,R} - \mathbf{U}_{i+1/2,L})$$

where $\mathbf{F}_{i+1/2,L}$ and $\mathbf{U}_{i+1/2,L}$ are formed from $[\rho, u, v, w, P]_{i+1/2,L}$
and $\mathbf{F}_{i+1/2,R}$ and $\mathbf{U}_{i+1/2,R}$ are formed from $[\rho, u, v, w, P]_{i+1/2,R}$

Primitive variable reconstruction for generic flow variable φ (no slope limiting)

UBR-3 $\varphi_{i+1/2,L} = (-\varphi_{i-1} + 5\varphi_i + 2\varphi_{i+1})/6$

UBR-5 $\varphi_{i+1/2,L} = (4\varphi_{i-2} - 26\varphi_{i-1} + 94\varphi_i + 54\varphi_{i+1} - 6\varphi_{i+2})/120$

UBR-7 $\varphi_{i+1/2,L} = (-6\varphi_{i-3} + 50\varphi_{i-2} - 202\varphi_{i-1} + 638\varphi_i + 428\varphi_{i+1} - 76\varphi_{i+2} + 8\varphi_{i+3})/840$

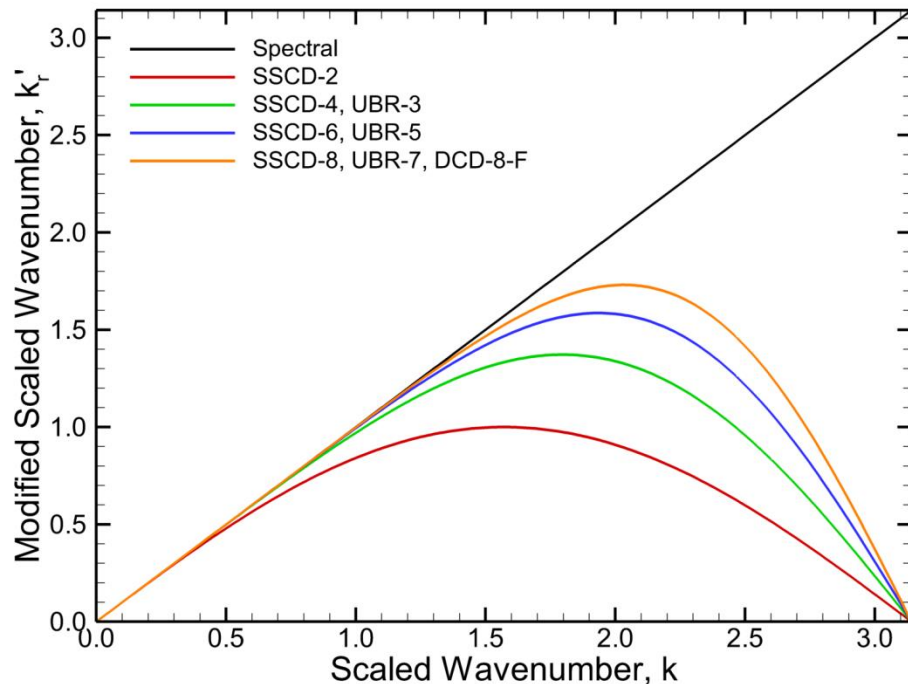
The $\varphi_{i+1/2,R}$ values are formed from a flipped interpolation

Note: none of the inviscid flux schemes used here, including the upwind-biased methods, should be considered as “shock-capturing” (i.e. MUSCL or WENO methods)

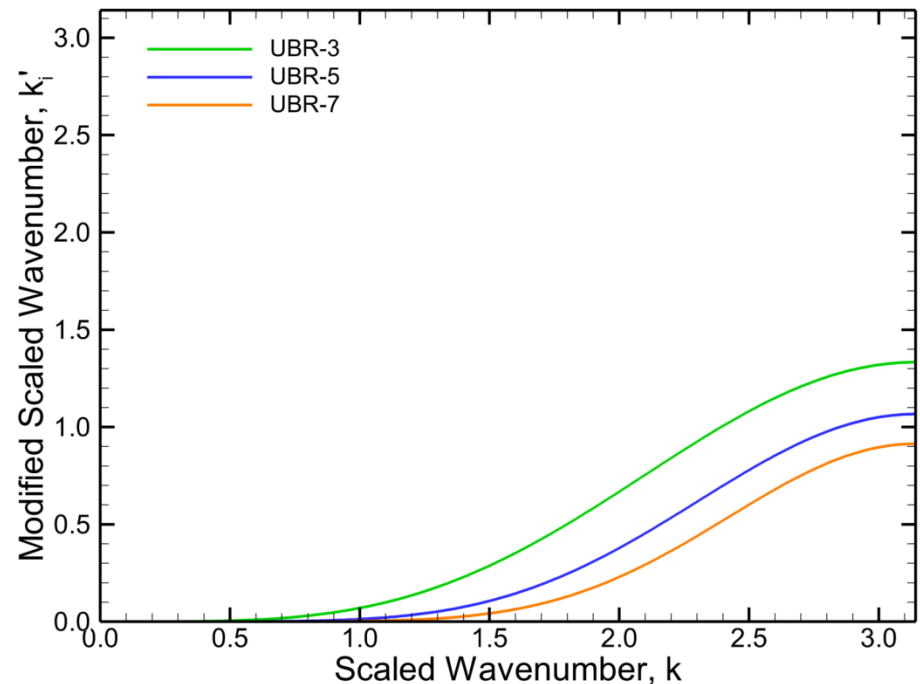


Fourier Analysis Characteristics

Real Part of Modified Scaled Wave-number: Dispersion (Phase)



Imaginary Part of Modified Scaled Wave-number: Dissipation



- ◆ The dispersion (phase) characteristics of each UBR scheme are the same as the SSCD/DCD scheme of one higher order of accuracy
- ◆ SSCD-2 has a limited range of phase accuracy, higher-order schemes get progressively better
- ◆ Central schemes are non-dissipative, while all upwind schemes experience increasing dissipation error at higher wavenumbers
- ◆ Higher-order upwind schemes have smaller dissipation error at lower wavenumbers than lower-order upwind schemes



Additional Numerical Details

Air at $T_\infty = 298.15$ K, $R = 287$ J/Kg-K, $\gamma = 1.4$, $c_p = 1004.5$ J/Kg-K,
 $a_\infty = 346.117$ m/s, $\mu =$ Sutherland relation, $\lambda =$ Sutherland relation

Domain: $0 \leq x \leq 9.6L$, $0 \leq y \leq 10L$, $0 \leq z \leq 4.8L$, $L = 0.01$ m

Grid A: $128 \times 97 \times 128$

Grid B: $192 \times 129 \times 192$

Grid C: $256 \times 145 \times 256$

uniform spacing and periodic B.Cs. in x- and z-directions

nonuniform spacing and adiabatic viscous wall B.C. (lower boundary) and
non-reflecting characteristic B.C. (upper boundary) in y-direction

4-stage Runge-Kutta time advancement

Initial condition obtained from prescribed turbulent mean flow profile and
velocity fluctuations obtained from channel flow simulations (see paper)



Summary of Freestream Conditions and Cases Run

Nominal Reynolds Number Cases

U_∞ (m/s)	M_∞	P_∞ (Pa)	Re_∞ (m^{-1})	SSCD				UBR			DCD-8-F
				-2	-4	-6	-8	-3	-5	-7	
50	0.144	25331	8.05×10^5	B	B	B	B	B	B	B	B
250	0.722	5066	8.05×10^5	B	B	B	B	B	B	B	B
500	1.445	3800	1.21×10^6				A			A	
				B	B	B	B	B	B	B	B
							C			C	
750	2.167	3800	1.81×10^6				A			A	
				B	B	B	B	B	B	B	B
							C			C	
1000	2.889	4560	2.90×10^6				A			A	
				B	B	B	B	B	B	B	B
							C			C	

Grid A = $128 \times 97 \times 128$ $\Delta y_w^+ \approx 0.33$, $\Delta x^+ \approx 24$, $\Delta z^+ \approx 12$

Grid B = $192 \times 129 \times 192$ $\Delta y_w^+ \approx 0.33$, $\Delta x^+ \approx 16$, $\Delta z^+ \approx 8$

Grid C = $256 \times 145 \times 256$ $\Delta y_w^+ \approx 0.33$, $\Delta x^+ \approx 12$, $\Delta z^+ \approx 6$

Note: only
SSCD-8 and
UBR-7 were run
on grids A and C



Summary of Freestream Conditions and Cases Run

Nominal Reynolds Numbers Cases (Cont'd)

U_∞ (m/s)	M_∞	P_∞ (Pa)	Re_∞ (m^{-1})	SSCD				UBR			DCD-8-F
				-2	-4	-6	-8	-3	-5	-7	
1250	3.612	5066	4.03×10^6							A	
						B	B	B	B	B	B
							C			C	
1500	4.334	6333	6.04×10^6							A	
								B	B	B	B
										C	
1750	5.056	7599	8.46×10^6							A	
								B	B	B	B
										C	

Note: only SSCD-8 and UBR-7 were run on grids A and C

Grid A = $128 \times 97 \times 128$ $\Delta y_w^+ \approx 0.33$, $\Delta x^+ \approx 24$, $\Delta z^+ \approx 12$

Grid B = $192 \times 129 \times 192$ $\Delta y_w^+ \approx 0.33$, $\Delta x^+ \approx 16$, $\Delta z^+ \approx 8$

Grid C = $256 \times 145 \times 256$ $\Delta y_w^+ \approx 0.33$, $\Delta x^+ \approx 12$, $\Delta z^+ \approx 6$



Summary of Freestream Conditions and Cases Run

Reduced Reynolds Number Cases

U_∞ (m/s)	M_∞	P_∞ (Pa)	Re_∞ (m^{-1})	SSCD				UBR			DCD-8-F
				-2	-4	-6	-8	-3	-5	-7	
500	1.445	2533	8.05×10^5				A			A	
							B			B	
							C			C	
750	2.167	2533	1.21×10^6				A			A	
							B			B	
							C			C	
1000	2.889	3040	1.93×10^6				A			A	
							B			B	
							C			C	

Note: only SSCD-8 and UBR-7 were run at these conditions

Grid A = $128 \times 97 \times 128$ $\Delta y_w^+ \approx 0.23$, $\Delta x^+ \approx 16$, $\Delta z^+ \approx 8$

Grid B = $192 \times 129 \times 192$ $\Delta y_w^+ \approx 0.22$, $\Delta x^+ \approx 11$, $\Delta z^+ \approx 5$

Grid C = $256 \times 145 \times 256$ $\Delta y_w^+ \approx 0.22$, $\Delta x^+ \approx 8$, $\Delta z^+ \approx 4$



Summary of Freestream Conditions and Cases Run

Reduced Reynolds Number Cases (Cont'd)

U_∞ (m/s)	M_∞	P_∞ (Pa)	Re_∞ (m^{-1})	SSCD				UBR			DCD-8-F
				-2	-4	-6	-8	-3	-5	-7	
1250	3.612	3378	2.68×10^6				A			A	
							B			B	
							C			C	
1500	4.334	4222	4.03×10^6							A	
							B			B	
							C			C	
1750	5.056	5066	5.64×10^6							A	
										B	
										C	

Note: only SSCD-8 and UBR-7 were run at these conditions

Grid A = $128 \times 97 \times 128$ $\Delta y_w^+ \approx 0.23$, $\Delta x^+ \approx 16$, $\Delta z^+ \approx 8$

Grid B = $192 \times 129 \times 192$ $\Delta y_w^+ \approx 0.22$, $\Delta x^+ \approx 11$, $\Delta z^+ \approx 5$

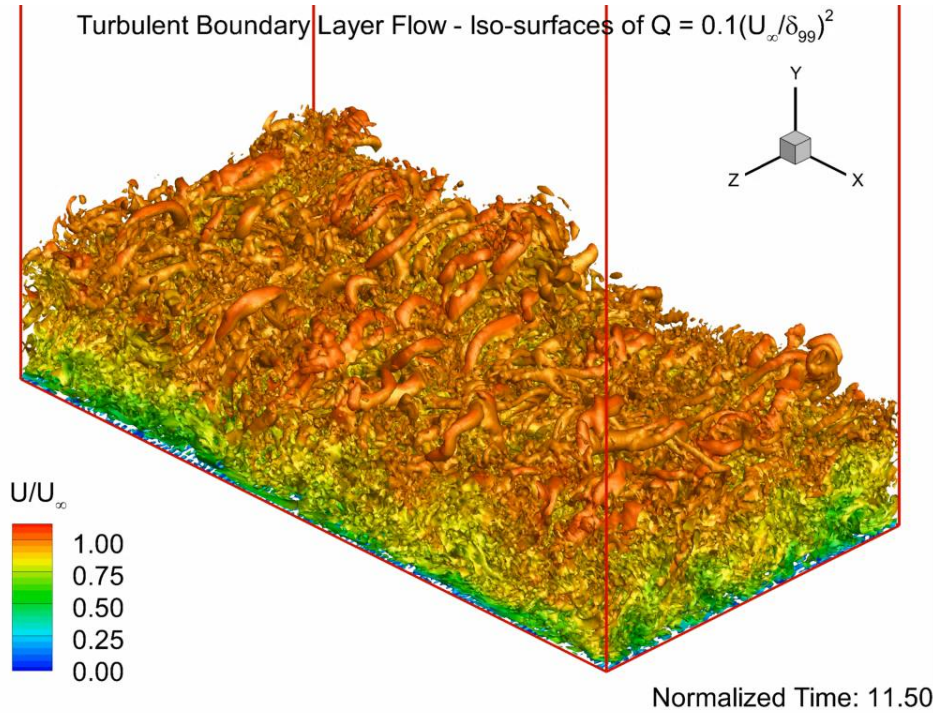
Grid C = $256 \times 145 \times 256$ $\Delta y_w^+ \approx 0.22$, $\Delta x^+ \approx 8$, $\Delta z^+ \approx 4$



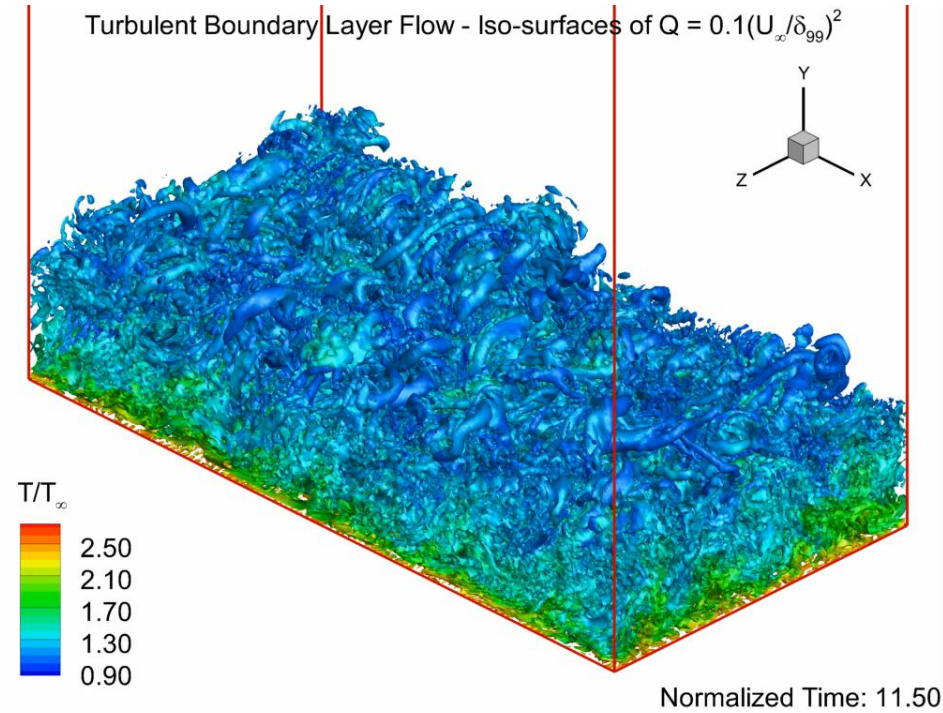
Turbulent Boundary Layer at Mach 2.889, $Re = 1.93 \times 10^6 \text{ m}^{-1}$

Iso-surfaces of Q-criterion

Normalized Velocity



Normalized Temperature



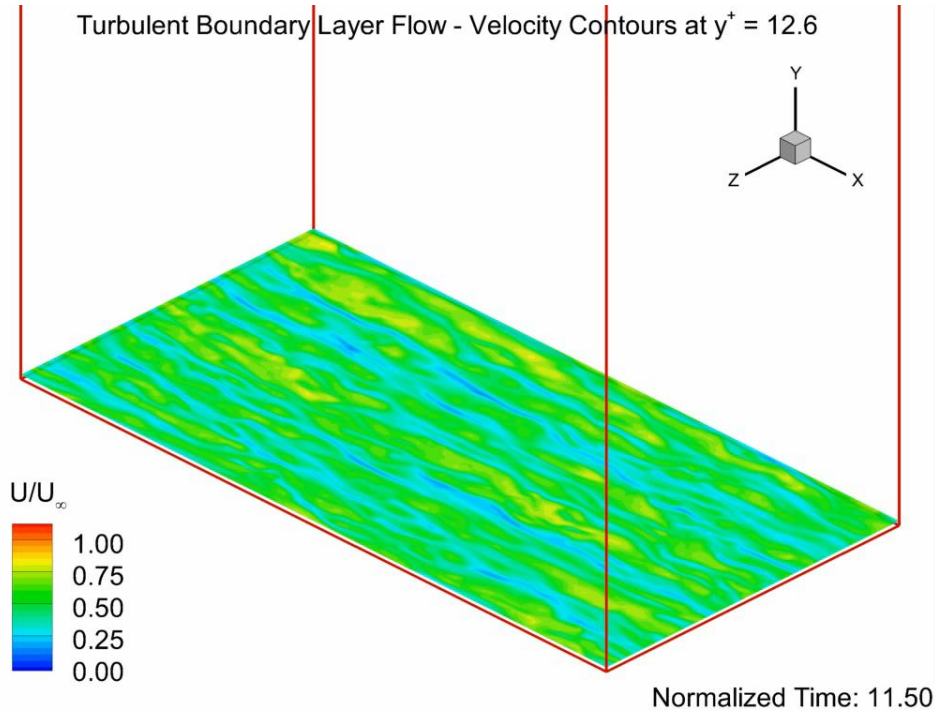
- ◆ Simulation run using SSCD-8 scheme on Grid C: $256 \times 145 \times 256$ points
- ◆ Iso-surfaces colored by normalized velocity magnitude U/U_∞ and temperature T/T_∞
- ◆ t^* is a normalized timescale $t U_\infty / 9.6L$ (domain flowthrough timescale)
- ◆ Turbulent flow structure is evident, as are sharp gradients near wall



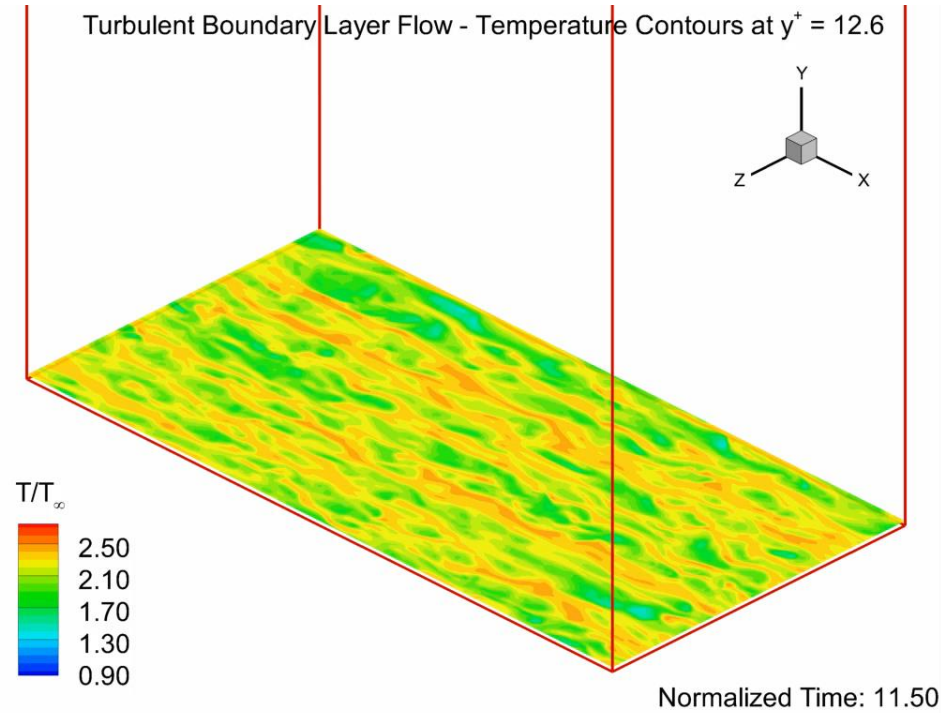
Turbulent Boundary Layer at Mach 2.889, $Re = 1.93 \times 10^6 \text{ m}^{-1}$

Contour Plots in x-z plane at $y^+ = 12.6$

Normalized Velocity



Normalized Temperature



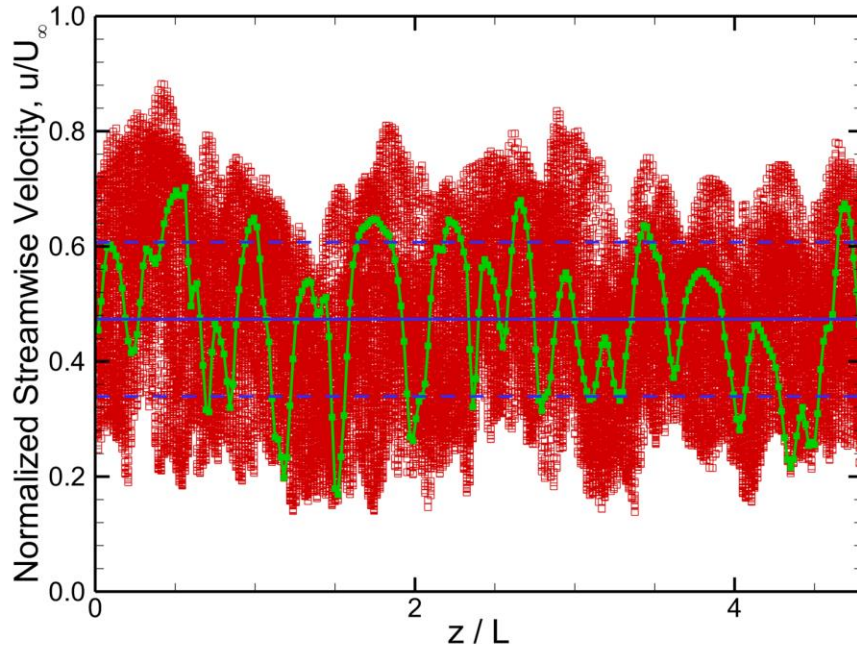
- ◆ Velocity magnitude and temperature are normalized by freestream values
- ◆ This x-z cutting lane at $y^+ = 12.6$ is the location of peak velocity fluctuations
- ◆ Elongated streaky structures characteristic of near-wall turbulence are easily observed, along with sharp fluctuations in temperature



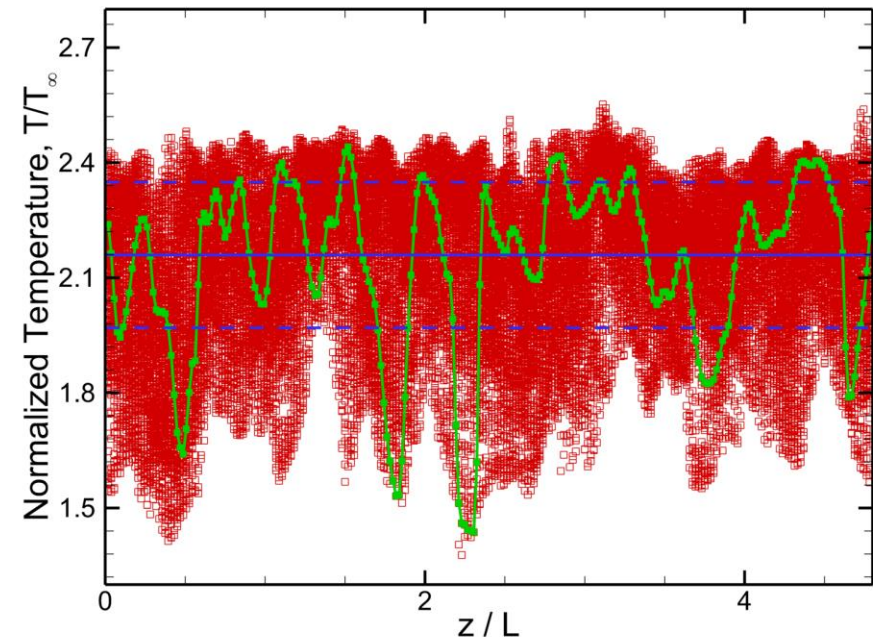
Turbulent Boundary Layer at Mach 2.889, $Re = 1.93 \times 10^6 \text{ m}^{-1}$

Scatter Plots in x-z plane at $y^+ = 12.6$

Normalized Streamwise Velocity



Normalized Temperature



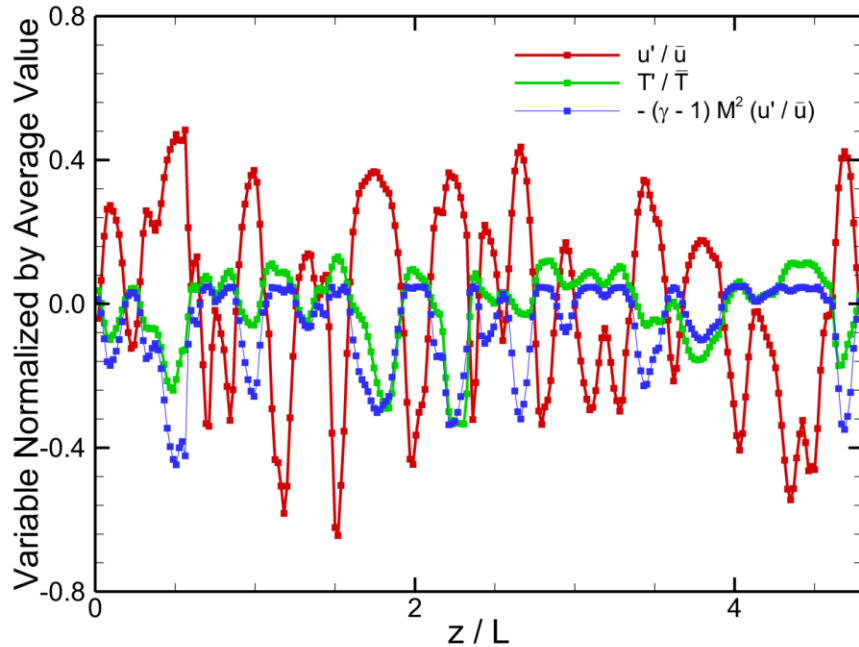
- ◆ Streamwise velocity and temperature are normalized by freestream values
- ◆ The green line and symbols indicates a results extracted from a single line at $x / L = 4.8$
- ◆ The blue lines indicate the average value as well as \pm one standard deviation
- ◆ The streaky structures are quite evident in the constant x-station spanwise profiles
- ◆ As the calculation of the inviscid flux involves computing derivatives of variables involving ρ , u , v , w and p , the need for adequate grid resolution and high numerical accuracy in computing these types of flows is obvious



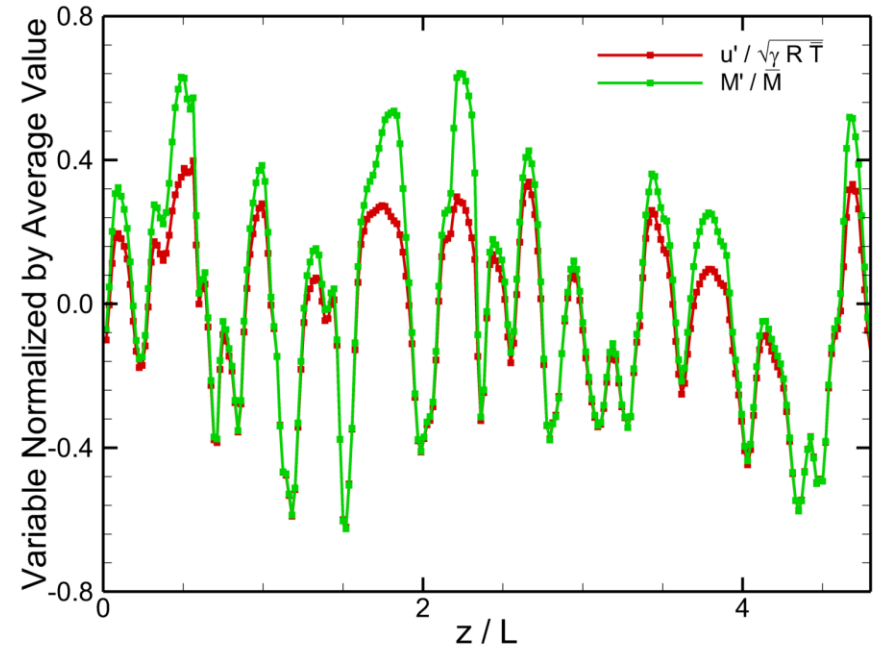
Turbulent Boundary Layer at Mach 2.889, $Re = 1.93 \times 10^6 \text{ m}^{-1}$

Normalized Fluctuations along $X / L = 4.8$ Line at $y^+ = 12.6$

Fluctuating u and T



Fluctuating Mach Numbers

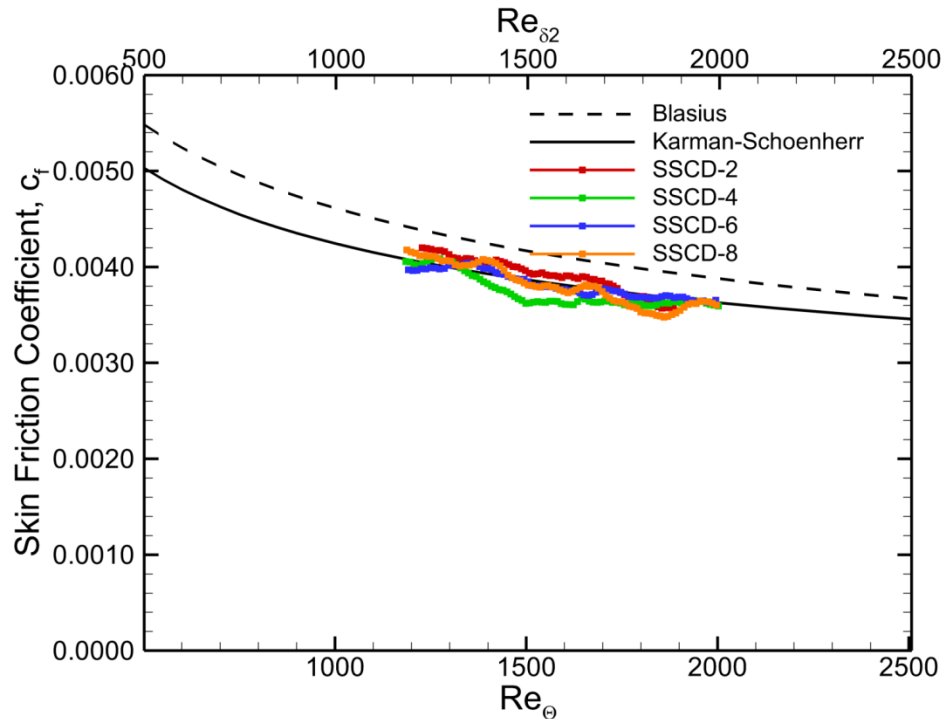


- ◆ In left panel, normalized streamwise velocity and temperature fluctuations are compared spanwise along the $x / L = 4.8$ line at $y^+ = 12.6$
- ◆ The two fluctuations are generally anti-correlated. Also shown is a plot of the “fluctuation” form of the Strong Reynolds Analogy for comparison. At the $y^+ = 12.6$ plane, the value of the RMS form of the SRA is 0.897 – a strong correlation on average.
- ◆ In the right panel, two expressions for the fluctuating Mach number are compared. The effect of the temperature/sound speed fluctuations (anti-correlated with u) is evident.

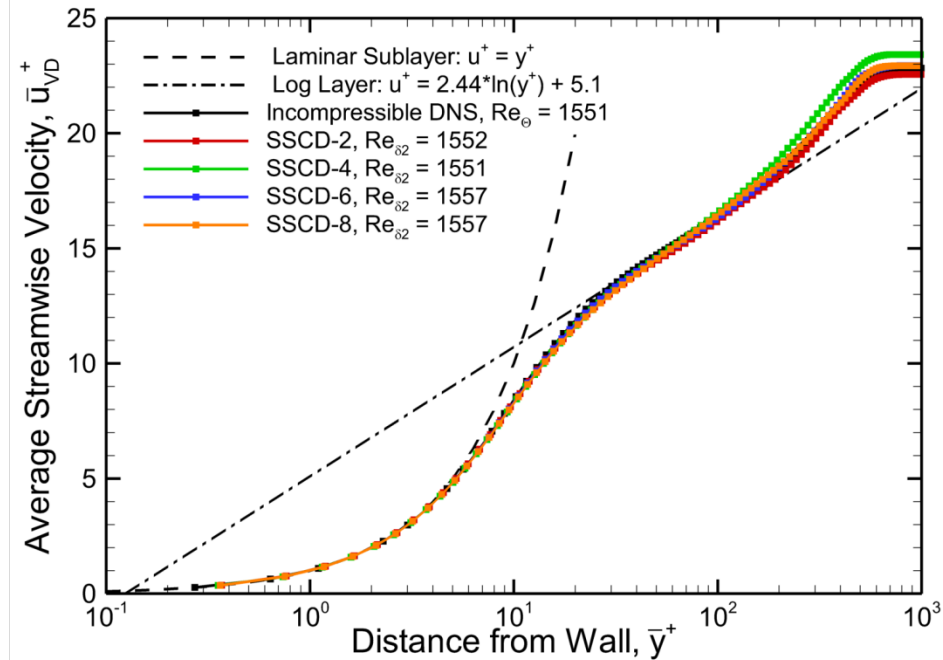


Comparison of Non-Dissipative SSCD Schemes at Mach 0.144, $Re = 8.05 \times 10^5 \text{ m}^{-1}$ on Grid B

Skin Friction



Mean Velocity Profiles (van Driest-transformed)

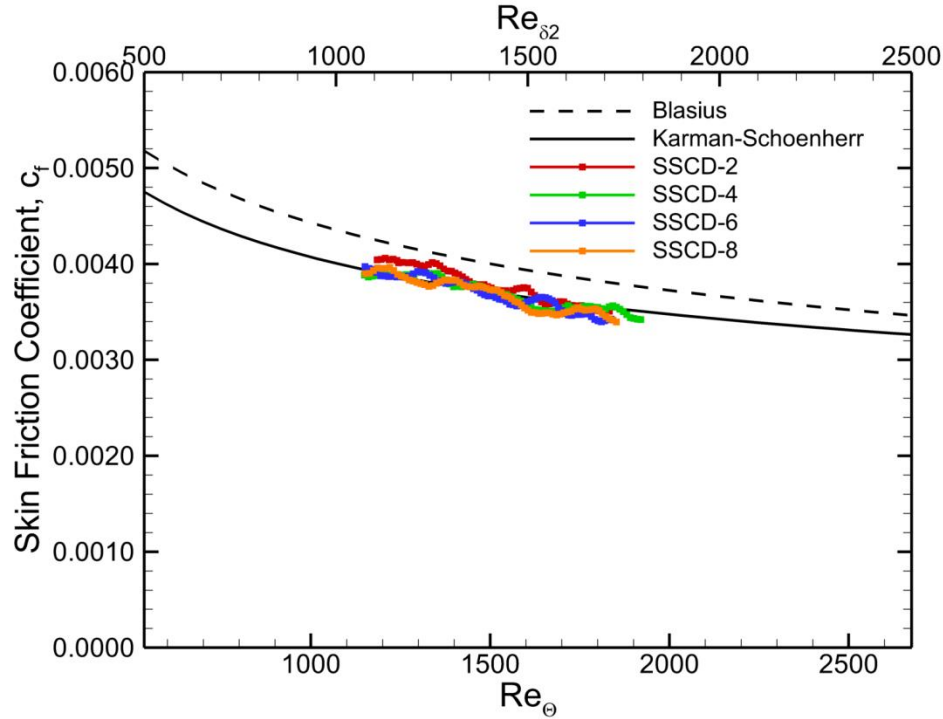


- ◆ All four SSCD schemes generally compare quite well with the transformed (van Driest II) Karman-Schoenherr relation for skin friction at this condition
- ◆ All four similarly match the laminar sublayer, log law, and incompressible DNS velocity profile of Simens et al. (2009) and Jimenez et al. (2010) at $Re_{\delta 2} = 1551$

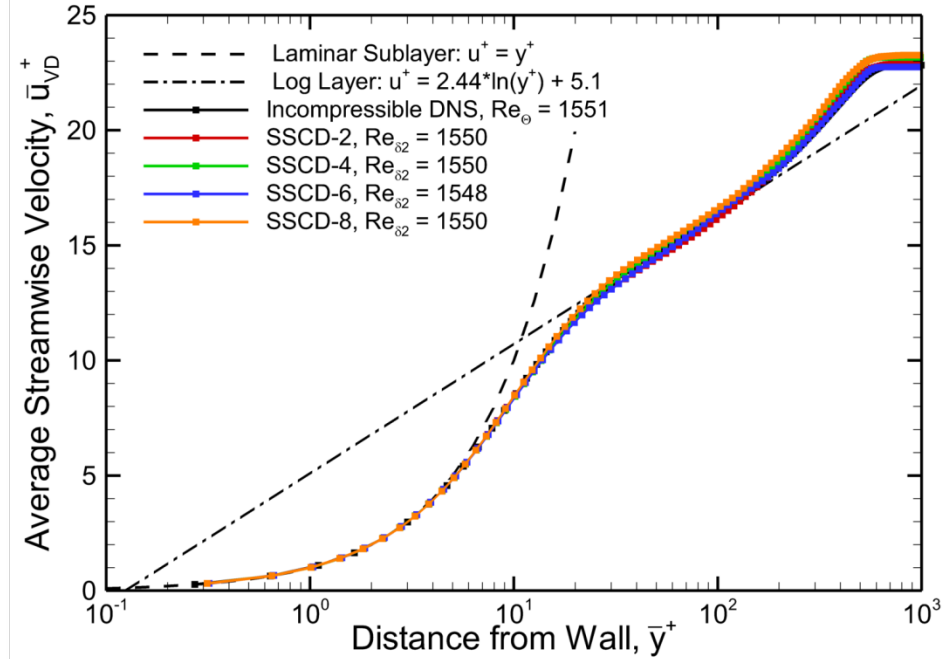


Comparison of Non-Dissipative SSCD Schemes at Mach 0.722, $Re = 8.05 \times 10^5 \text{ m}^{-1}$ on Grid B

Skin Friction



Mean Velocity Profiles (van Driest-transformed)

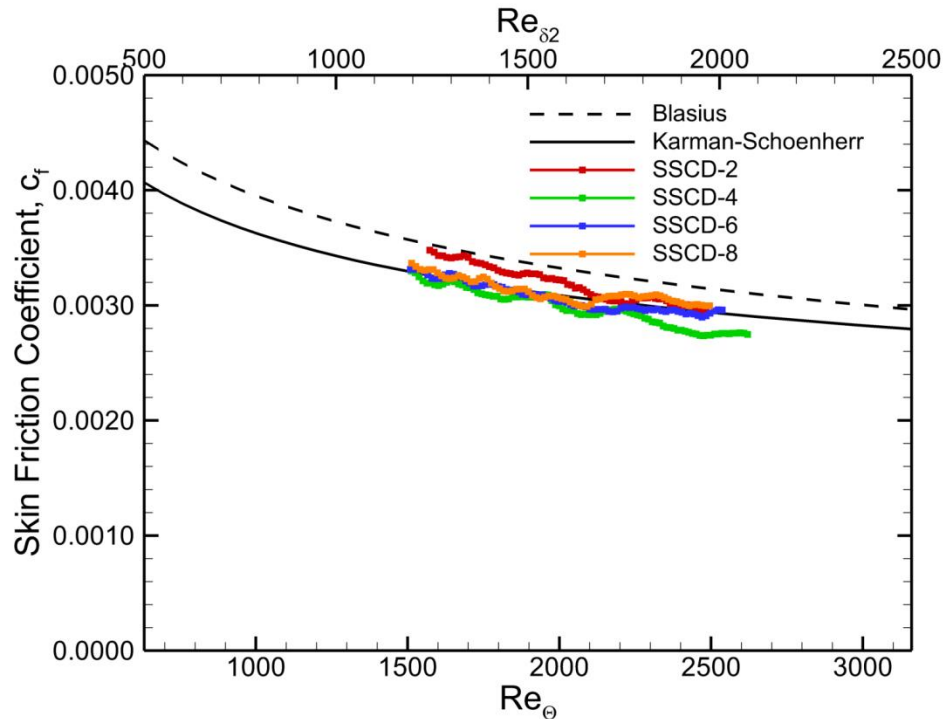


- ◆ All four SSCD schemes generally compare quite well with the transformed (van Driest II) Karman-Schoenherr relation for skin friction at this condition
- ◆ All four similarly match the laminar sublayer, log law, and incompressible DNS velocity profile at $Re_{\delta 2} = 1551$

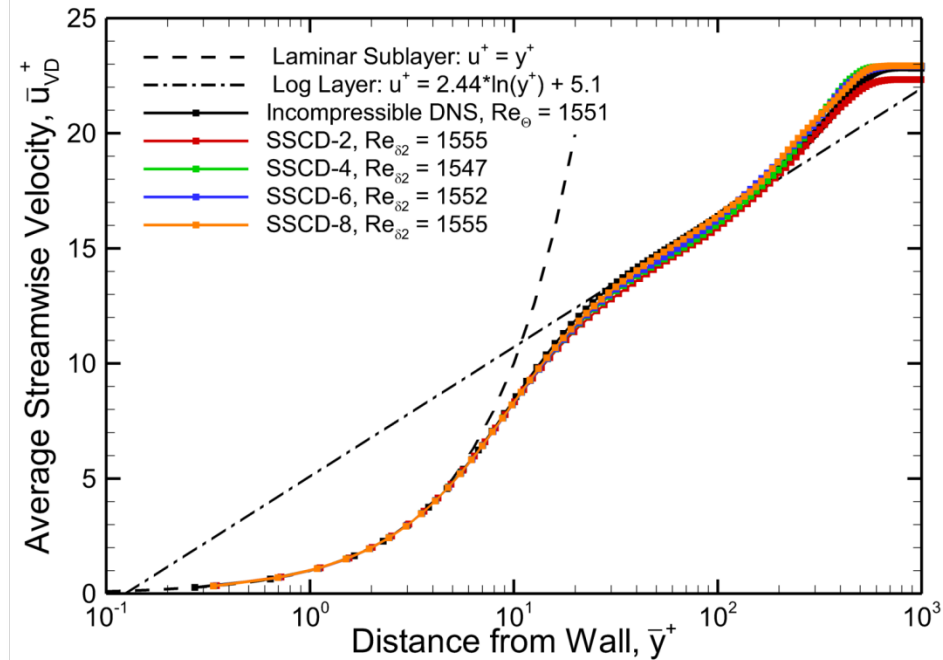


Comparison of Non-Dissipative SSCD Schemes at Mach 1.445, $Re = 1.21 \times 10^6 \text{ m}^{-1}$ on Grid B

Skin Friction



Mean Velocity Profiles (van Driest-transformed)

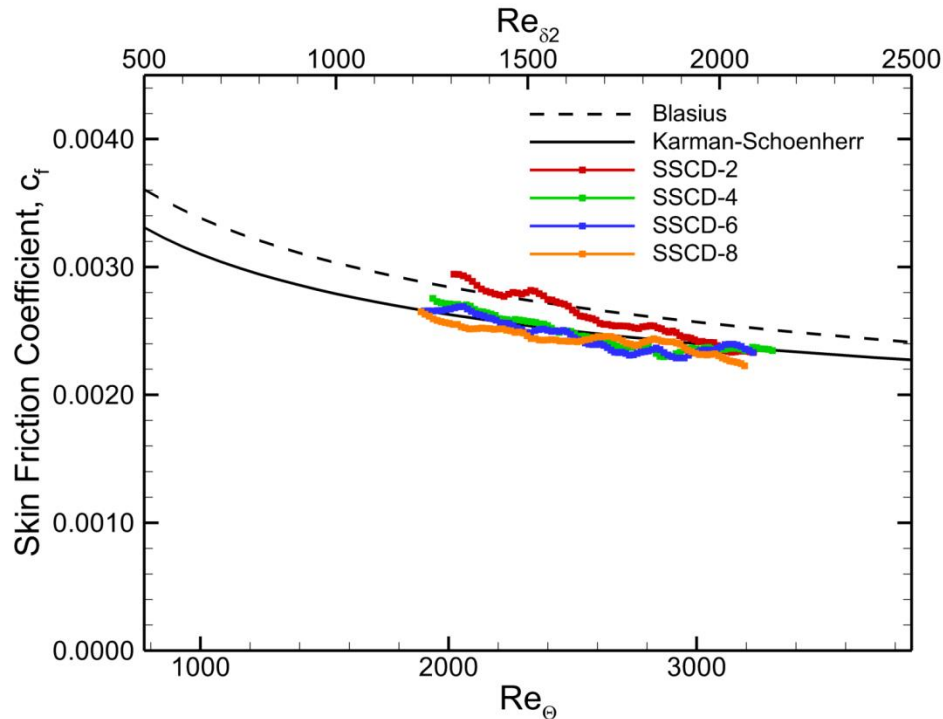


- ◆ The SSCD-4, -6 and -8 schemes generally compare quite well with the transformed (van Driest II) Karman-Schoenherr relation for skin friction at this condition. SSCD-2 exhibits a skin friction slightly higher than the relation.
- ◆ All three high-order methods similarly match the laminar sublayer, log law, and incompressible DNS velocity profile at $Re_{\delta 2} = 1551$. SSCD-2 begins to exhibit a slightly smaller wake strength than the others.

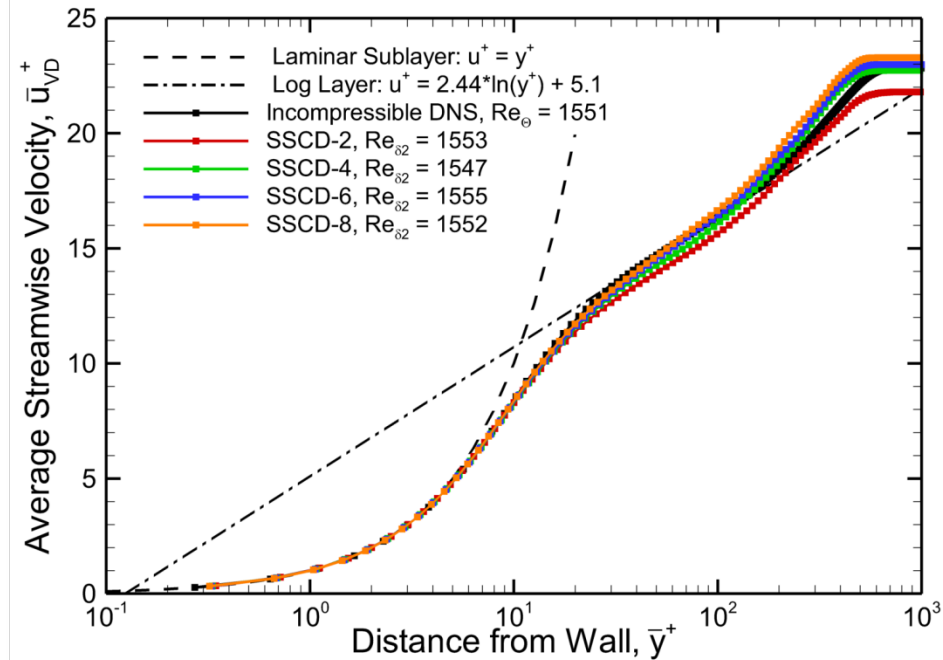


Comparison of Non-Dissipative SSCD Schemes at Mach 2.167, $Re = 1.81 \times 10^6 \text{ m}^{-1}$ on Grid B

Skin Friction



Mean Velocity Profiles (van Driest-transformed)

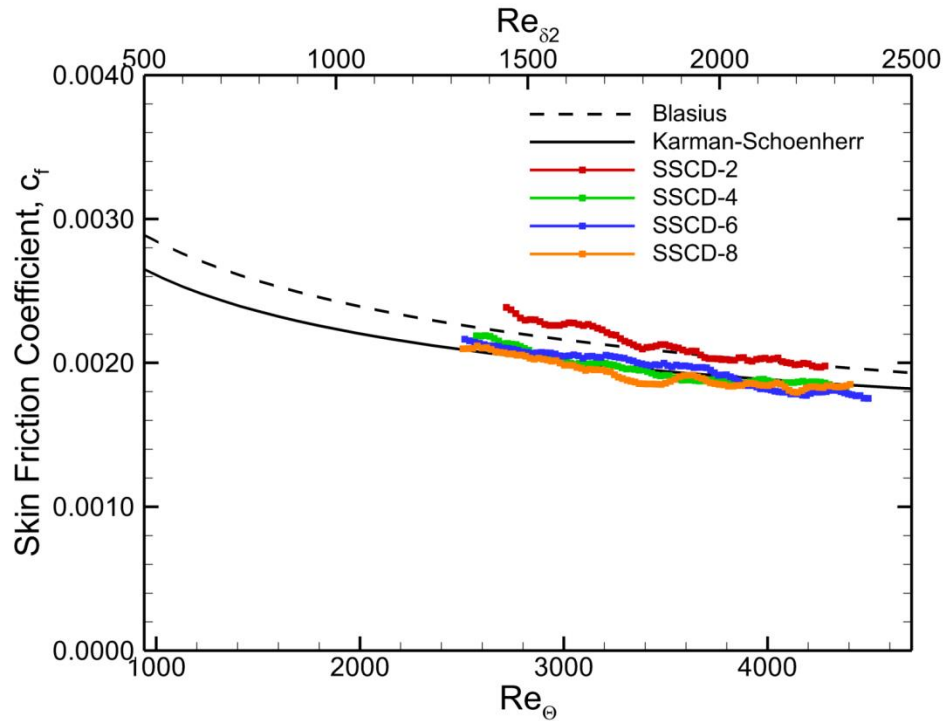


- ◆ The SSCD-4, -6 and -8 schemes generally compare quite well with the transformed (van Driest II) Karman-Schoenherr relation for skin friction at this condition. SSCD-2 exhibits a skin friction Re_θ higher than the relation.
- ◆ All three high-order methods similarly match the laminar sublayer, log law, and incompressible DNS velocity profile at $Re_{\delta_2} = 1551$. SSCD-2 exhibits a smaller wake strength than the others, and also starts to fall slightly below the log law line.

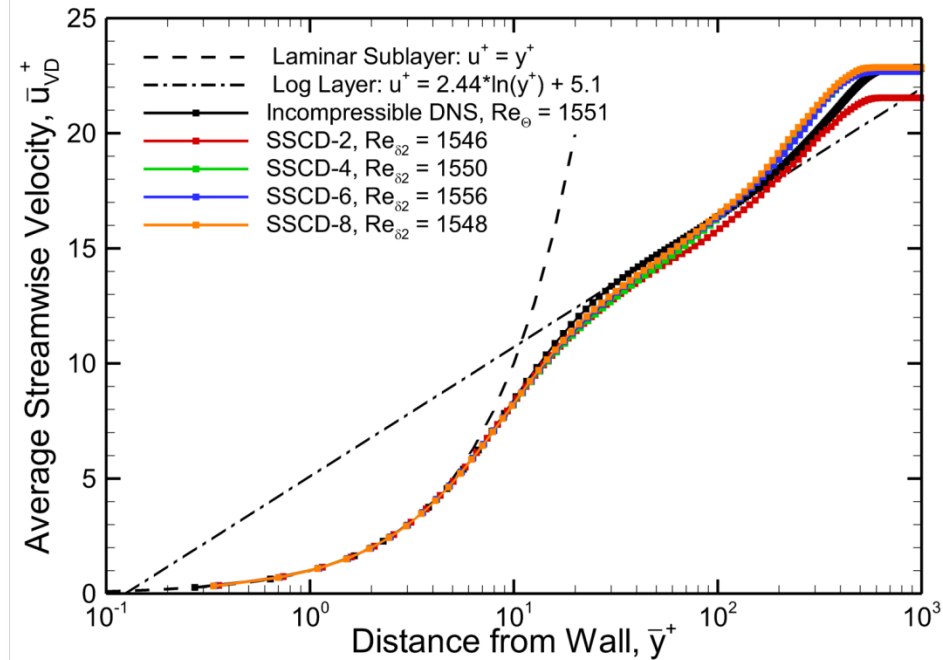


Comparison of Non-Dissipative SSCD Schemes at Mach 2.889, $Re = 2.90 \times 10^6 \text{ m}^{-1}$ on Grid B

Skin Friction



Mean Velocity Profiles (van Driest-transformed)

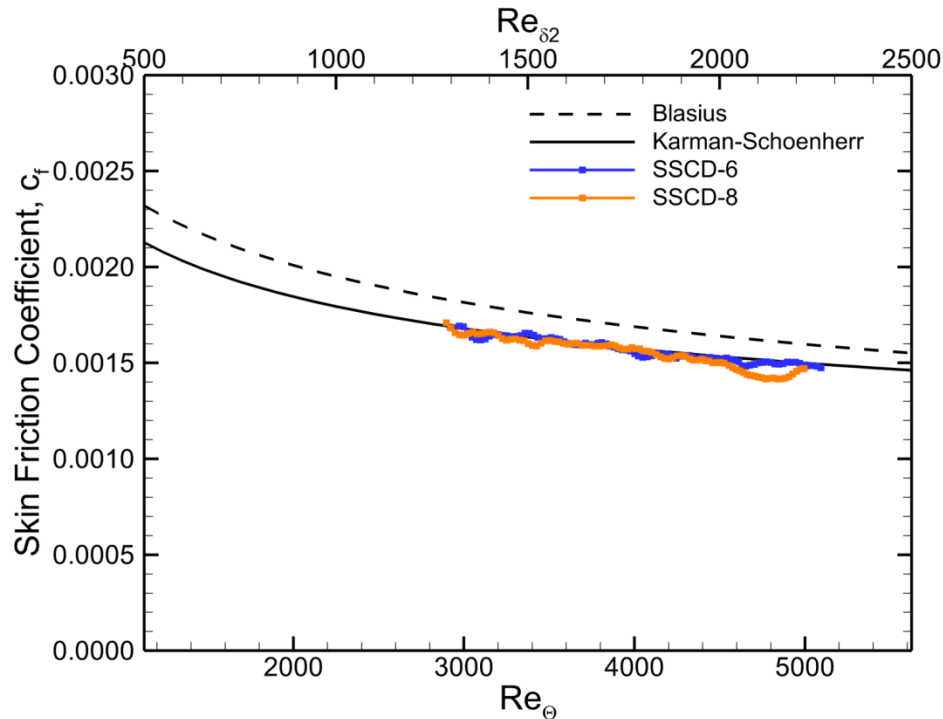


- ◆ The SSCD-4, -6 and -8 schemes generally compare quite well with the transformed (van Driest II) Karman-Schoenherr relation for skin friction at this condition. SSCD-2 exhibits a skin friction Re_θ higher than the relation.
- ◆ All three high-order methods similarly match the laminar sublayer, log law, and incompressible DNS velocity profile at $Re_{\delta_2} = 1551$. SSCD-2 exhibits a smaller wake strength than the others, and also starts to fall slightly below the log law line.

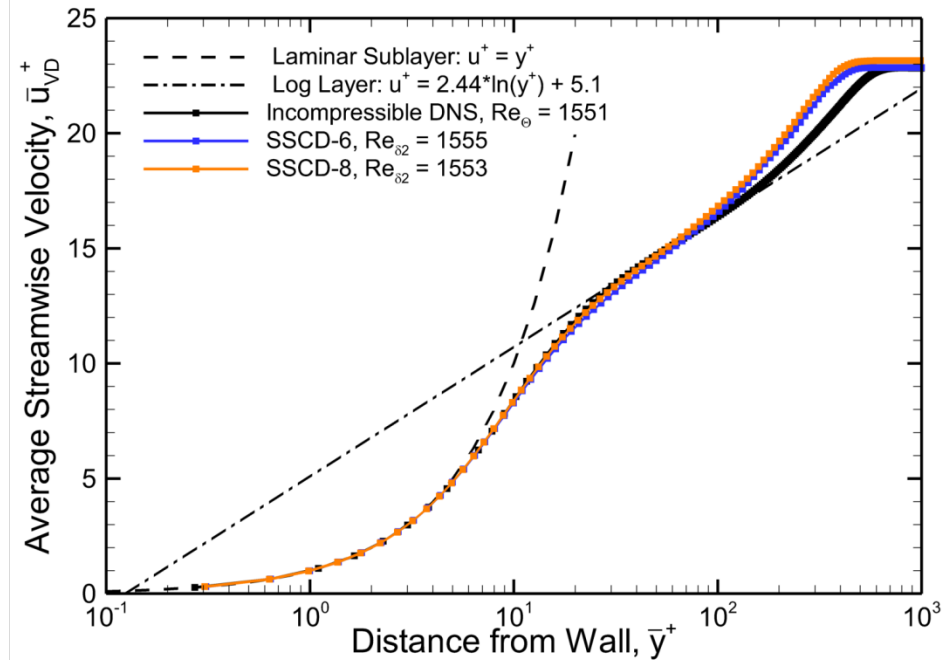


Comparison of Non-Dissipative SSCD Schemes at Mach 3.612, $Re = 4.03 \times 10^6 \text{ m}^{-1}$ on Grid B

Skin Friction



Mean Velocity Profiles (van Driest-transformed)

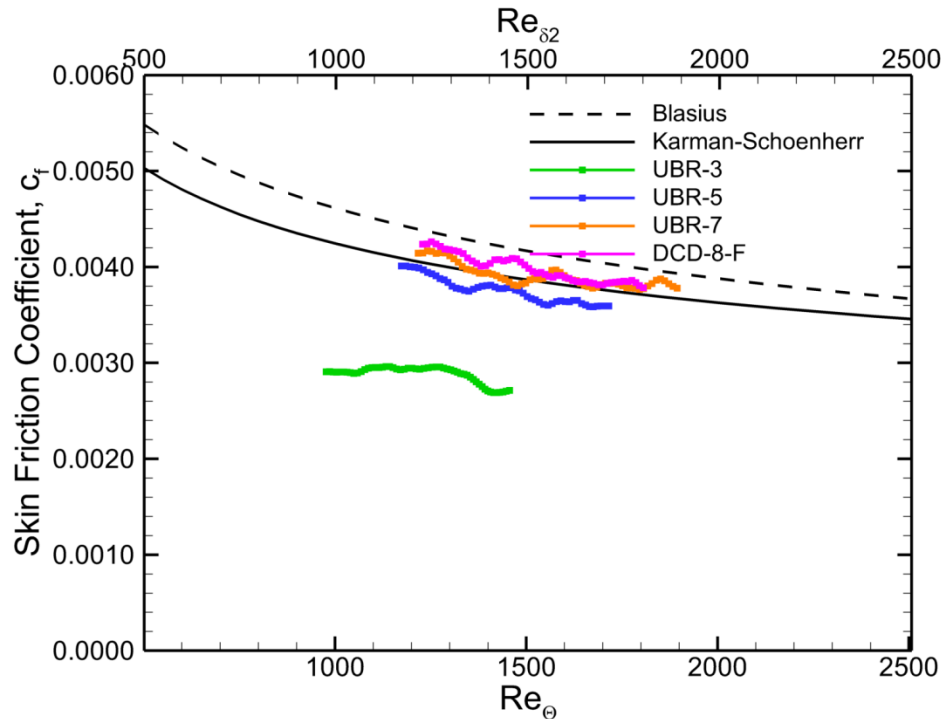


- ◆ The SSCD-6 and -8 schemes generally compare quite well with the transformed (van Driest II) Karman-Schoenherr relation for skin friction at this condition. SSCD-2 and -4 were not stable at this condition.
- ◆ The two high-order methods similarly match the laminar sublayer, log law, and incompressible DNS velocity profile at $Re_{\delta 2} = 1551$
- ◆ Note that the boundary layer thickness (at equivalent $Re_{\delta 2}$) has grown noticeably shorter in wall coordinates than was the case for the subsonic cases

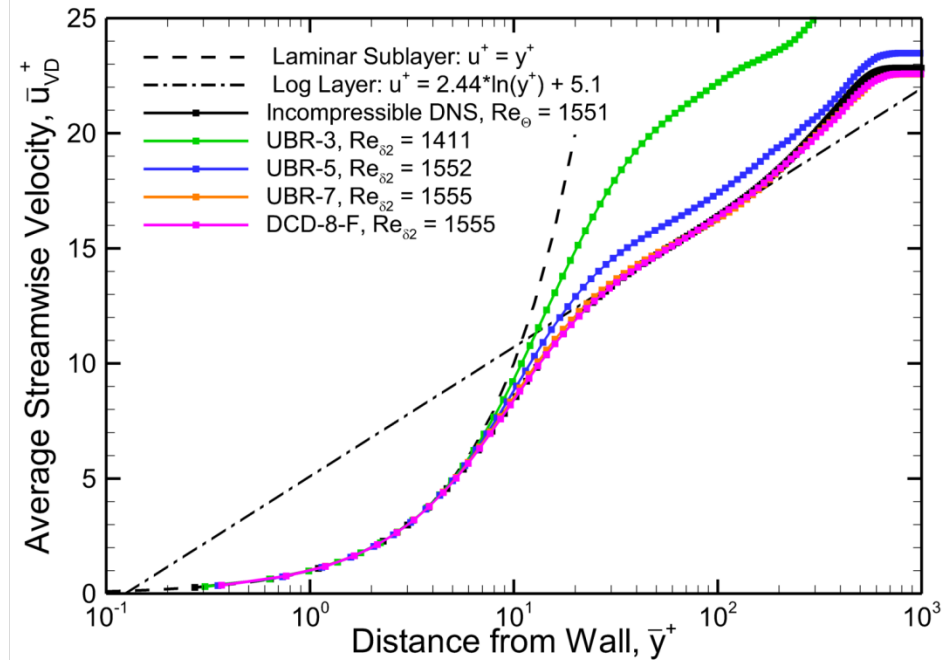


Comparison of Dissipative UBR and DCD-8-F Schemes at Mach 0.144, $Re = 8.05 \times 10^5 \text{ m}^{-1}$ on Grid B

Skin Friction



Mean Velocity Profiles (van Driest-transformed)

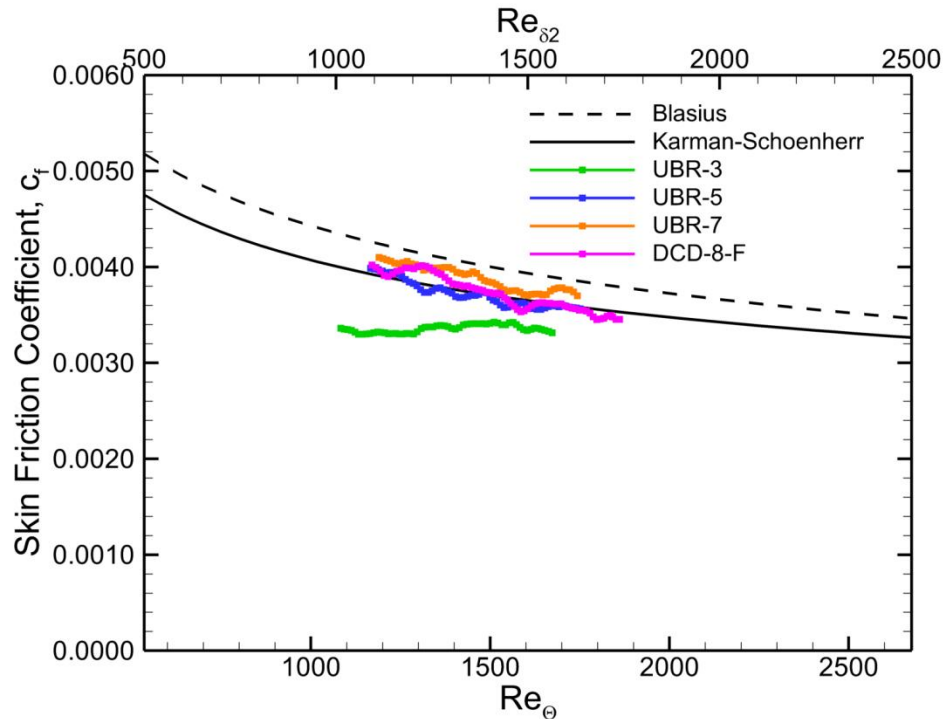


- ◆ The UBR-7 and DCD-8-F schemes generally compare quite well with the transformed (van Driest II) Karman-Schoenherr relation for skin friction at this condition
- ◆ They similarly match the laminar sublayer, log law, and incompressible DNS velocity profile at $Re_{\delta 2} = 1551$
- ◆ UBR-5 does less well, and UBR-3 does poorly. This can be traced to the excessive dissipation in the basic Roe scheme at low Mach numbers. Fixes for this published in recent years bring UBR-3 close to UBR-5 for this case.

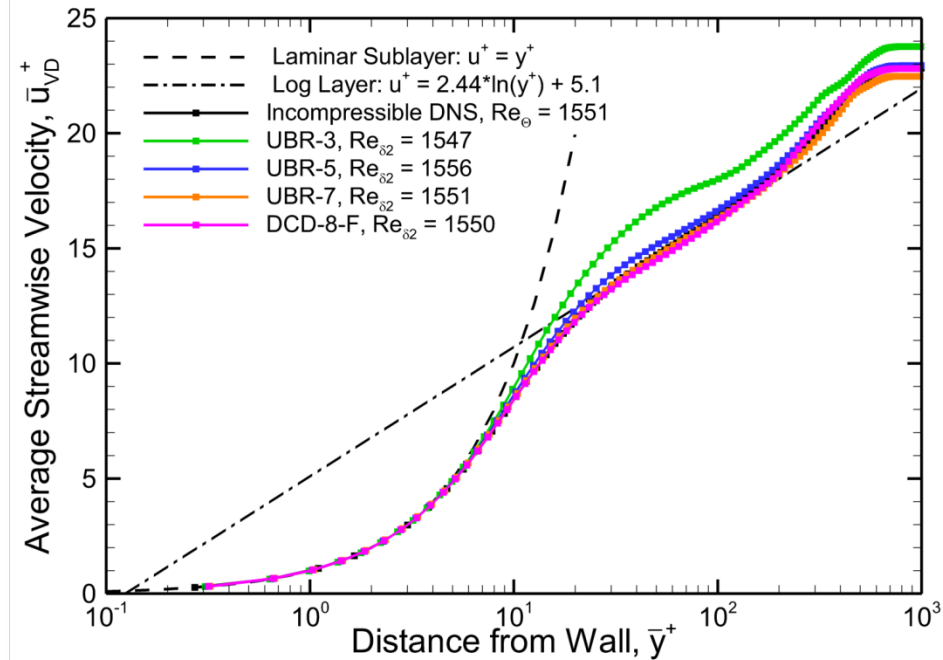


Comparison of Dissipative UBR and DCD-8-F Schemes at Mach 0.722, $Re = 8.05 \times 10^5 \text{ m}^{-1}$ on Grid B

Skin Friction



Mean Velocity Profiles (van Driest-transformed)

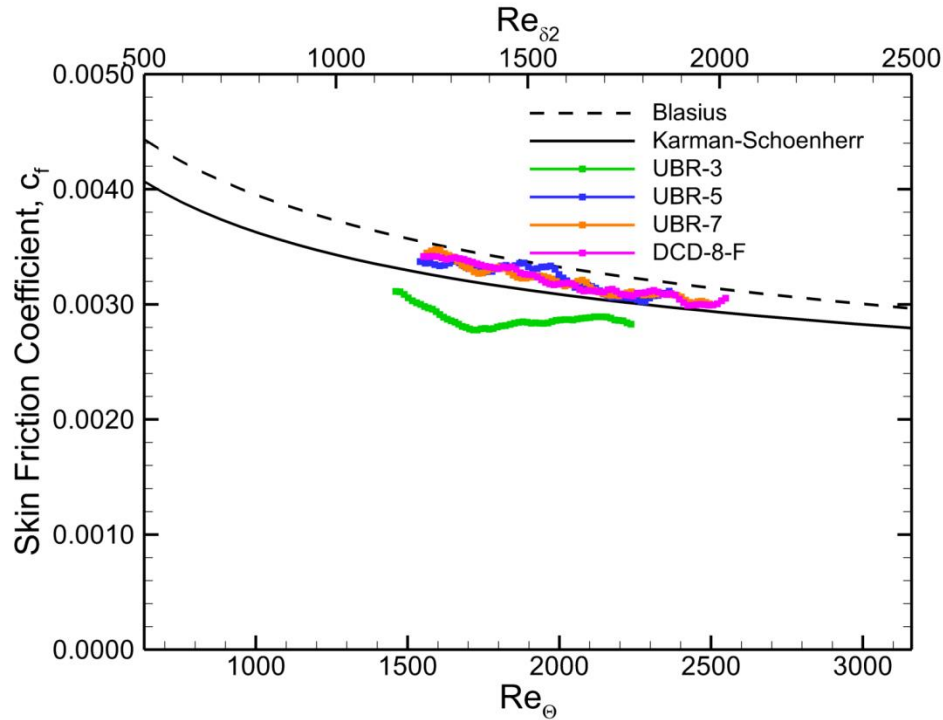


- ◆ The UBR-7 and DCD-8-F schemes generally compare quite well with the transformed (van Driest II) Karman-Schoenherr relation for skin friction at this condition
- ◆ They similarly match the laminar sublayer, log law, and incompressible DNS velocity profile at $Re_{\delta 2} = 1551$
- ◆ UBR-5 is now nearly as good as UBR-7 and DCD-8-F, rising slightly over the log law line
- ◆ UBR-3 is better than it was at Mach 0.144, but still has an unacceptable velocity profile

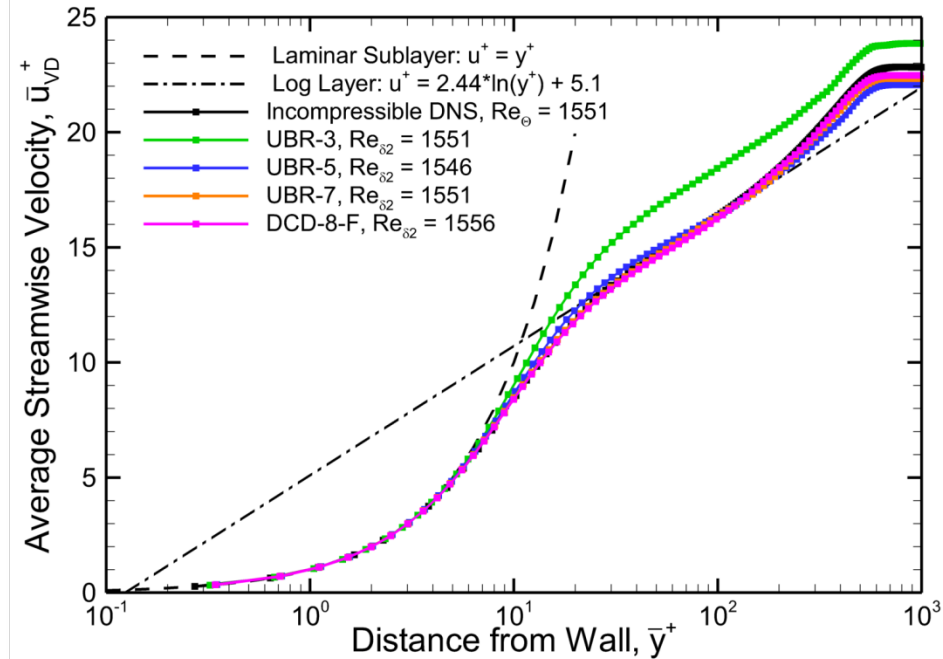


Comparison of Dissipative UBR and DCD-8-F Schemes at Mach 1.445, $Re = 1.21 \times 10^6 \text{ m}^{-1}$ on Grid B

Skin Friction



Mean Velocity Profiles (van Driest-transformed)

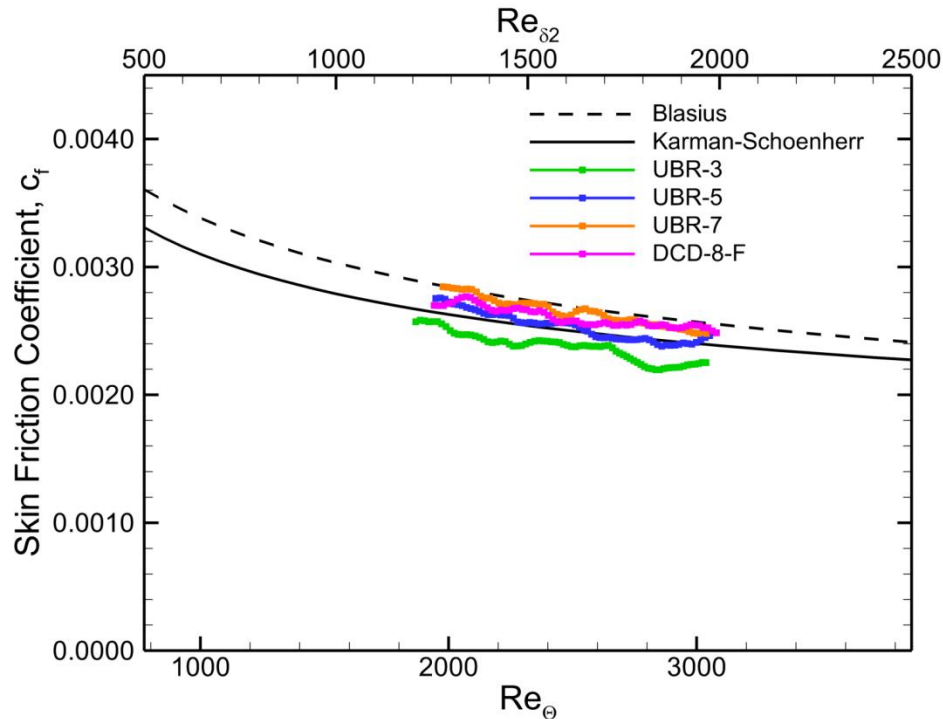


- ◆ The UBR-7 and DCD-8-F schemes generally compare quite well with the transformed (van Driest II) Karman-Schoenherr relation for skin friction at this condition
- ◆ They similarly match the laminar sublayer, log law, and incompressible DNS velocity profile at $Re_{\delta_2} = 1551$. Both do not predict quite the same wake strength that SSCD-8 did.
- ◆ UBR-5 is nearly as good as UBR-7 and DCD-8-F
- ◆ UBR-3 is better than it was at Mach 0.144, but still has an unacceptable velocity profile

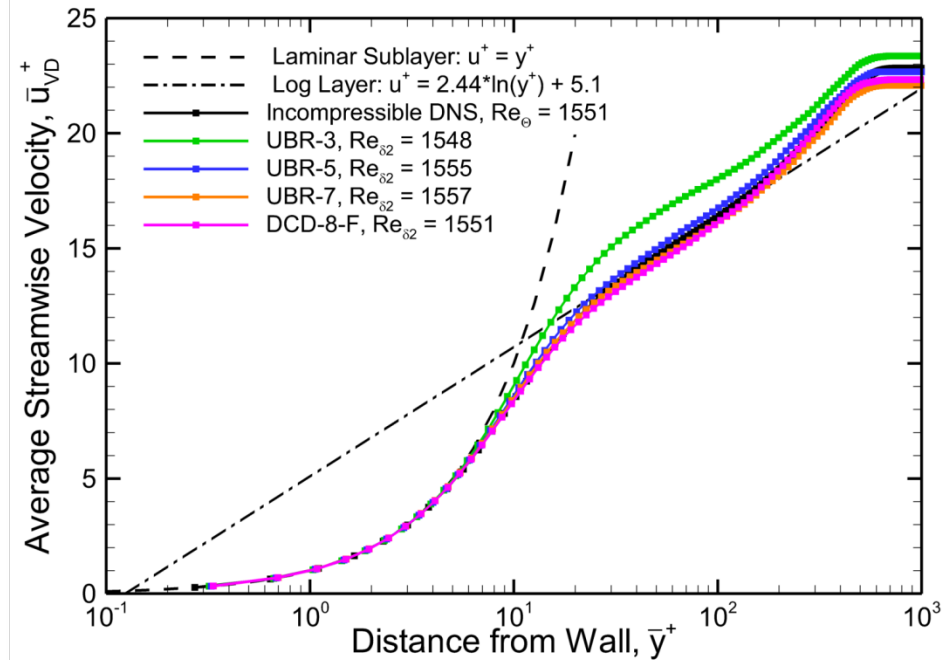


Comparison of Dissipative UBR and DCD-8-F Schemes at Mach 2.167, $Re = 1.81 \times 10^6 \text{ m}^{-1}$ on Grid B

Skin Friction



Mean Velocity Profiles (van Driest-transformed)

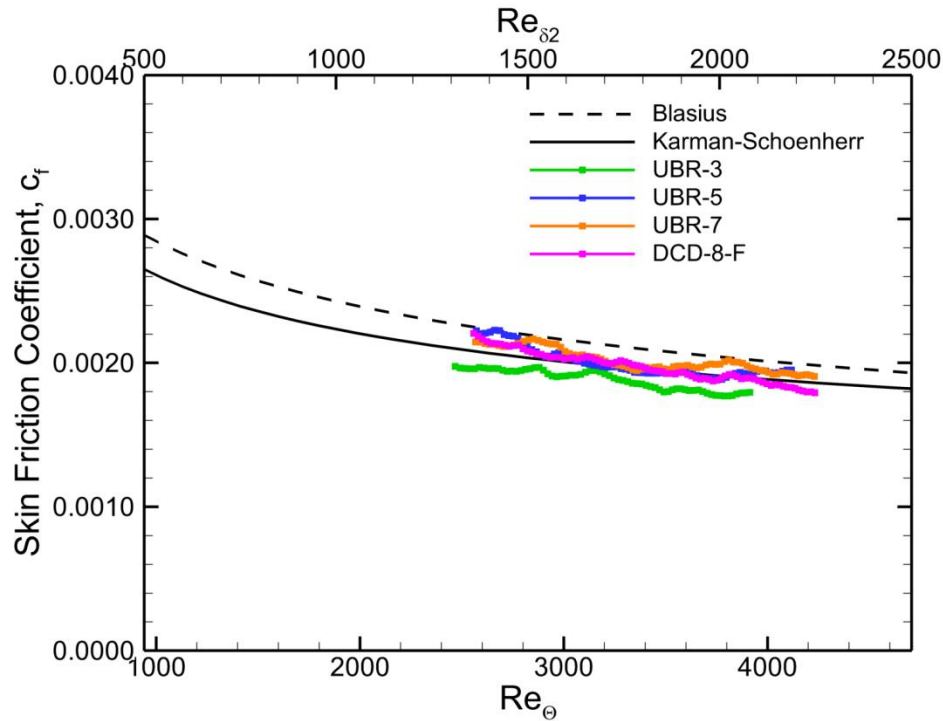


- ◆ The UBR-7 and DCD-8-F schemes generally compare well with the transformed (van Driest II) Karman-Schoenherr relation for skin friction at this condition
- ◆ They similarly match the laminar sublayer, log law, and incompressible DNS velocity profile at $Re_{\delta_2} = 1551$. Both do not predict quite the same wake strength that SSCD-8 did.
- ◆ UBR-5 is nearly as good as UBR-7 and DCD-8-F
- ◆ UBR-3 is better than it was at Mach 0.144, but still has an unacceptable velocity profile

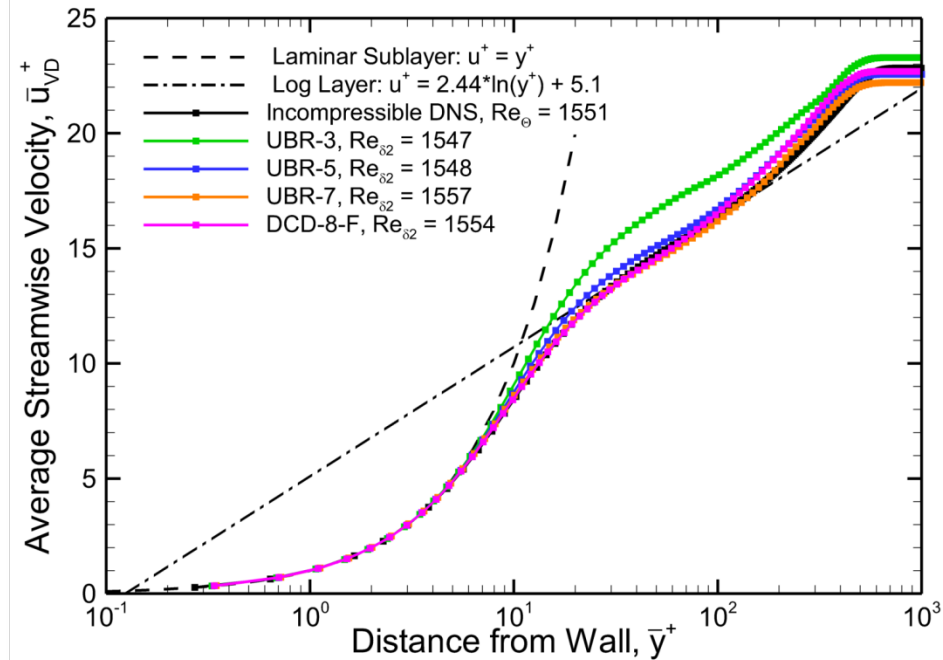


Comparison of Dissipative UBR and DCD-8-F Schemes at Mach 2.889, $Re = 2.90 \times 10^6 \text{ m}^{-1}$ on Grid B

Skin Friction



Mean Velocity Profiles (van Driest-transformed)

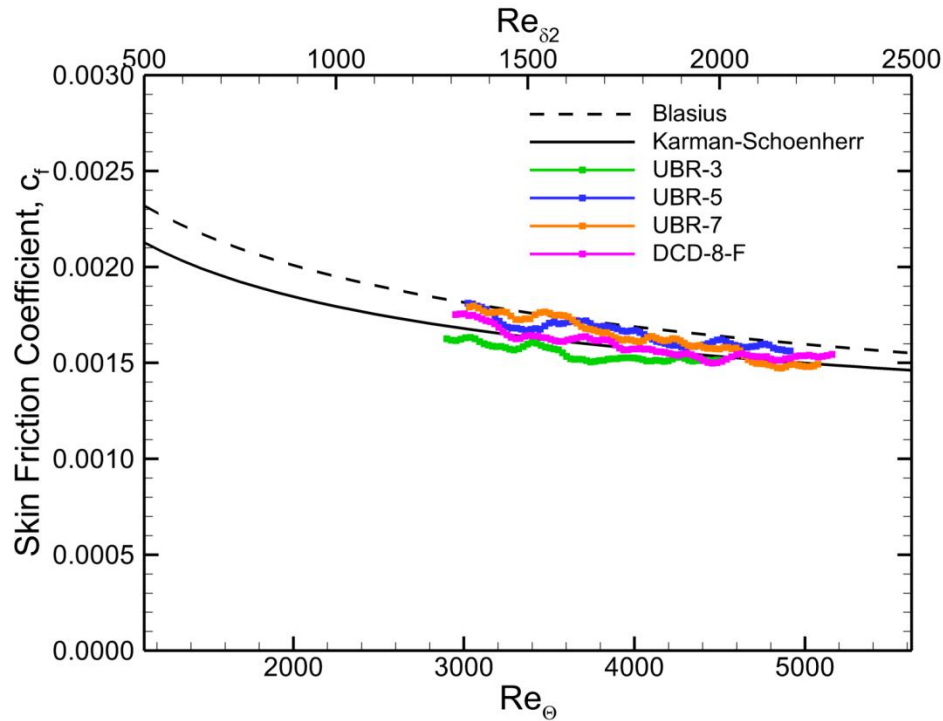


- ◆ The UBR-7 and DCD-8-F schemes generally compare quite well with the transformed (van Driest II) Karman-Schoenherr relation for skin friction at this condition
- ◆ They similarly match the laminar sublayer, log law, and incompressible DNS velocity profile at $Re_{\delta_2} = 1551$. UBR-7 does not predict quite the same wake strength that SSCD-8 did.
- ◆ UBR-5 is nearly as good as UBR-7 and DCD-8-F
- ◆ UBR-3 is better than it was at Mach 0.144, but still has an unacceptable velocity profile

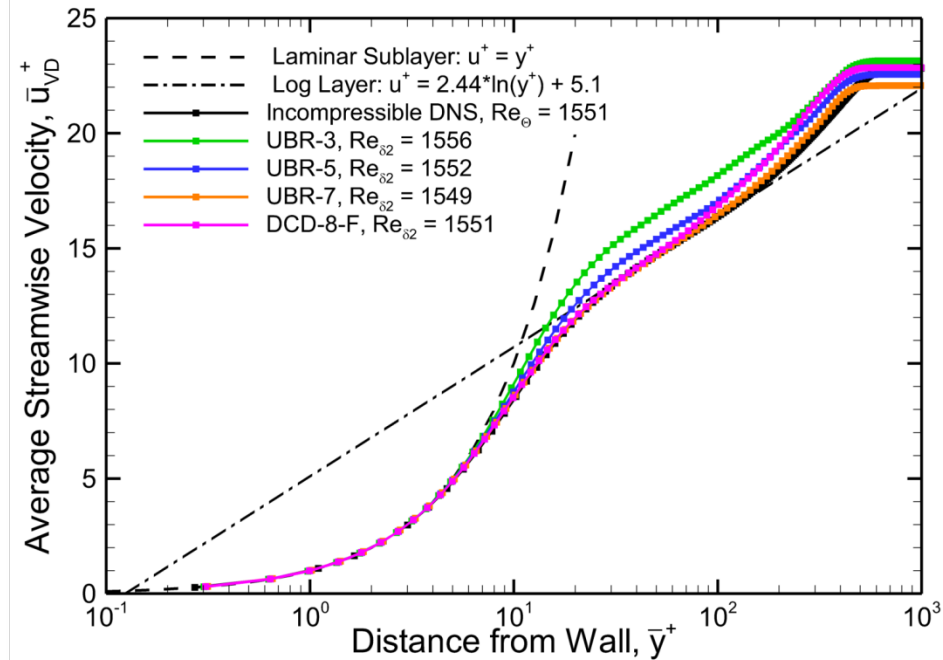


Comparison of Dissipative UBR and DCD-8-F Schemes at Mach 3.612, $Re = 4.03 \times 10^6 \text{ m}^{-1}$ on Grid B

Skin Friction



Mean Velocity Profiles (van Driest-transformed)

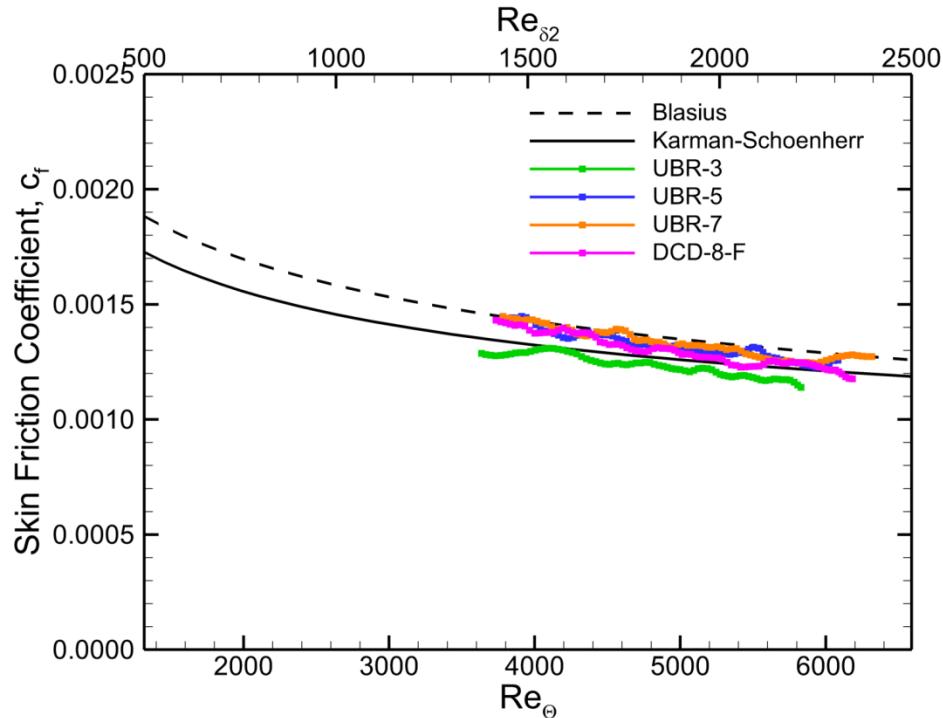


- ◆ The UBR-7 and DCD-8-F schemes generally compare quite well with the transformed (van Driest II) Karman-Schoenherr relation for skin friction at this condition
- ◆ They similarly match the laminar sublayer, log law, and incompressible DNS velocity profile at $Re_{\delta_2} = 1551$. UBR-7 does not predict quite the same wake strength that SSCD-8 did.
- ◆ UBR-5 is nearly as good as UBR-7 and DCD-8-F
- ◆ UBR-3 is better than it was at Mach 0.144, but still has an unacceptable velocity profile

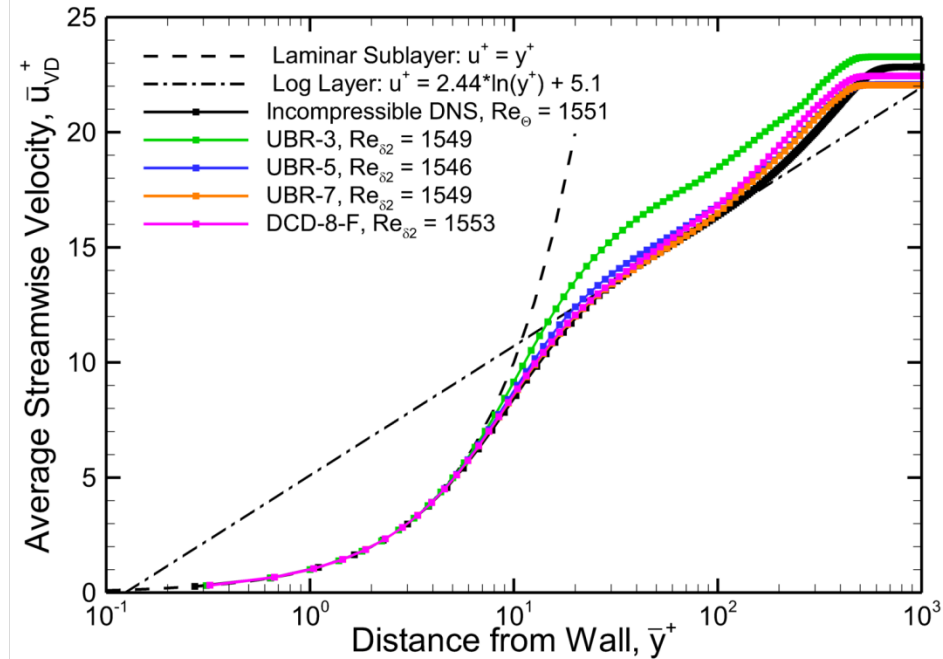


Comparison of Dissipative UBR and DCD-8-F Schemes at Mach 4.334, $Re = 6.04 \times 10^6 \text{ m}^{-1}$ on Grid B

Skin Friction



Mean Velocity Profiles (van Driest-transformed)

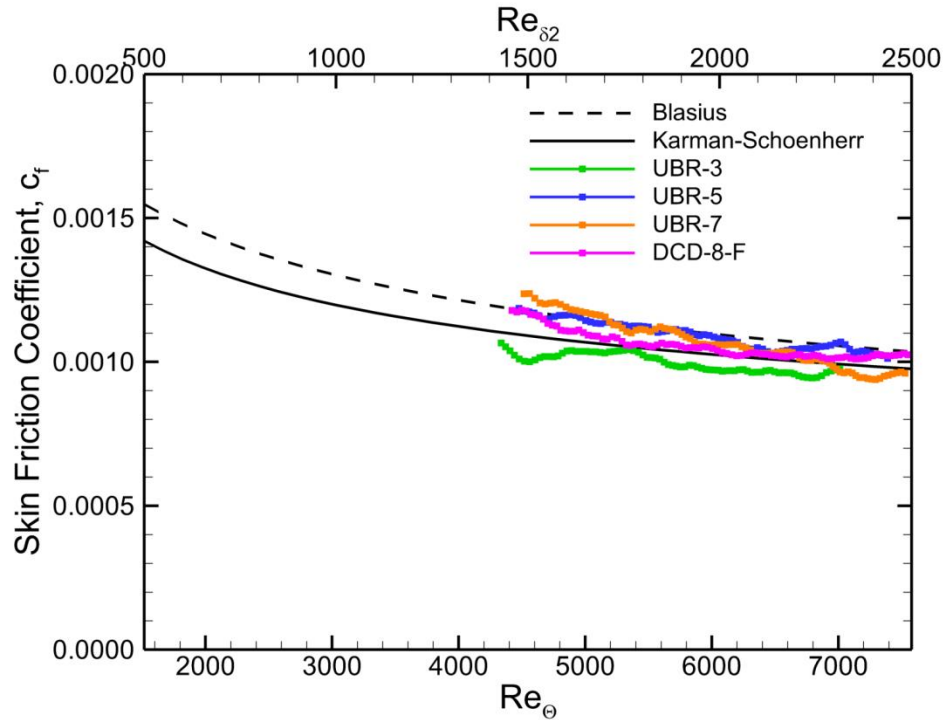


- ◆ The UBR-7 and DCD-8-F schemes generally compare quite well with the transformed (van Driest II) Karman-Schoenherr relation for skin friction at this condition
- ◆ They similarly match the laminar sublayer, log law, and incompressible DNS velocity profile at $Re_{\delta_2} = 1551$. DCD-8-F exhibits a slightly higher wake strength than UBR-7.
- ◆ UBR-5 is nearly as good as UBR-7 and DCD-8-F
- ◆ UBR-3 is better than it was at Mach 0.144, but still has an unacceptable velocity profile

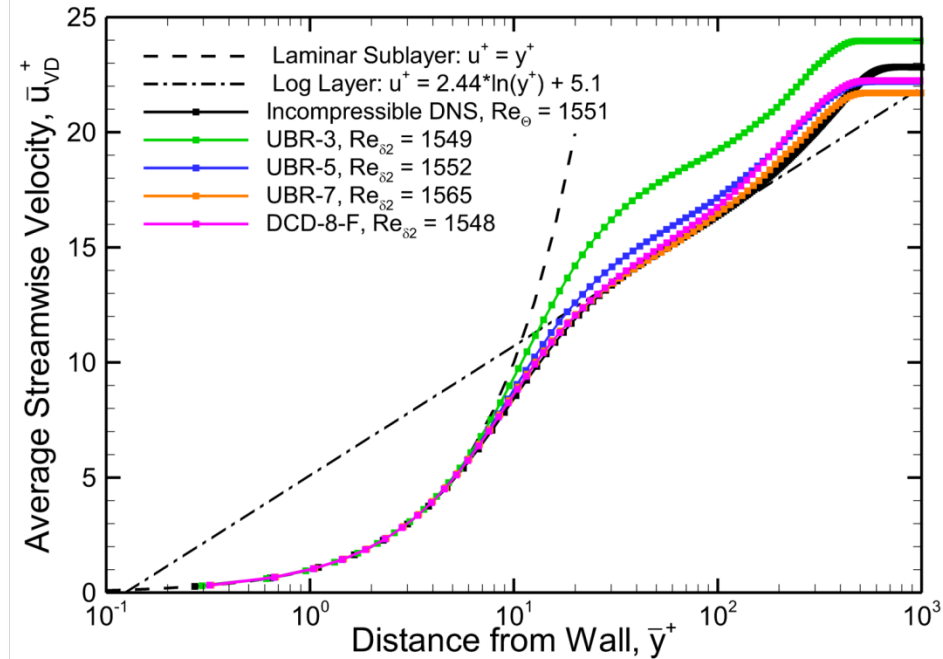


Comparison of Dissipative UBR and DCD-8-F Schemes at Mach 5.056, $Re = 8.46 \times 10^6 \text{ m}^{-1}$ on Grid B

Skin Friction



Mean Velocity Profiles (van Driest-transformed)

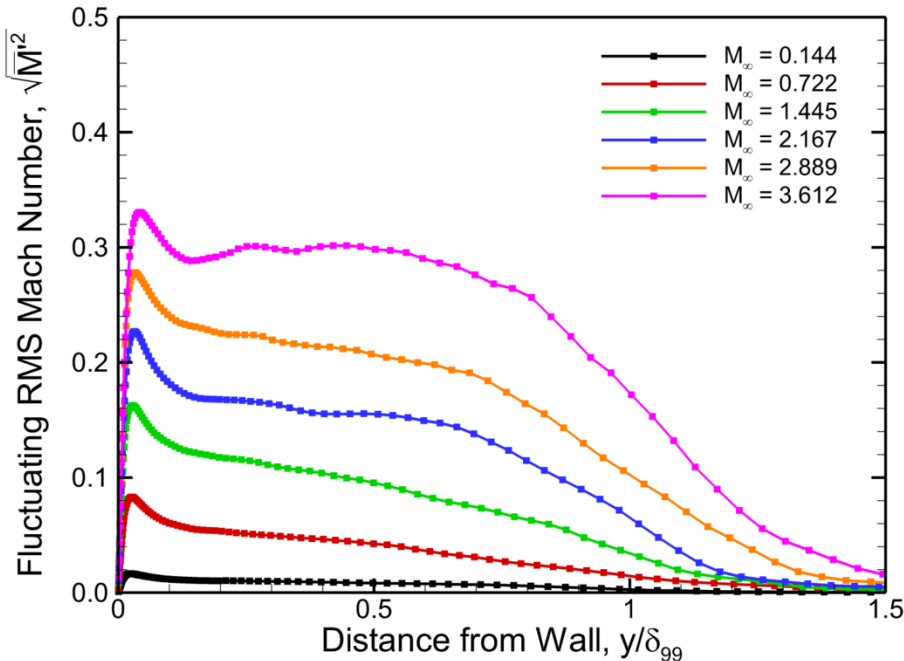


- ◆ The UBR-7 and DCD-8-F schemes generally compare quite well with the transformed (van Driest II) Karman-Schoenherr relation for skin friction at this condition
- ◆ They similarly match the laminar sublayer, log law, and incompressible DNS velocity profile at $Re_{\delta_2} = 1551$. DCD-8-F exhibits a slightly higher wake strength than UBR-7.
- ◆ UBR-5 is nearly as good as UBR-7 and DCD-8-F
- ◆ UBR-3 is better than it was at Mach 0.144, but still has an unacceptable velocity profile

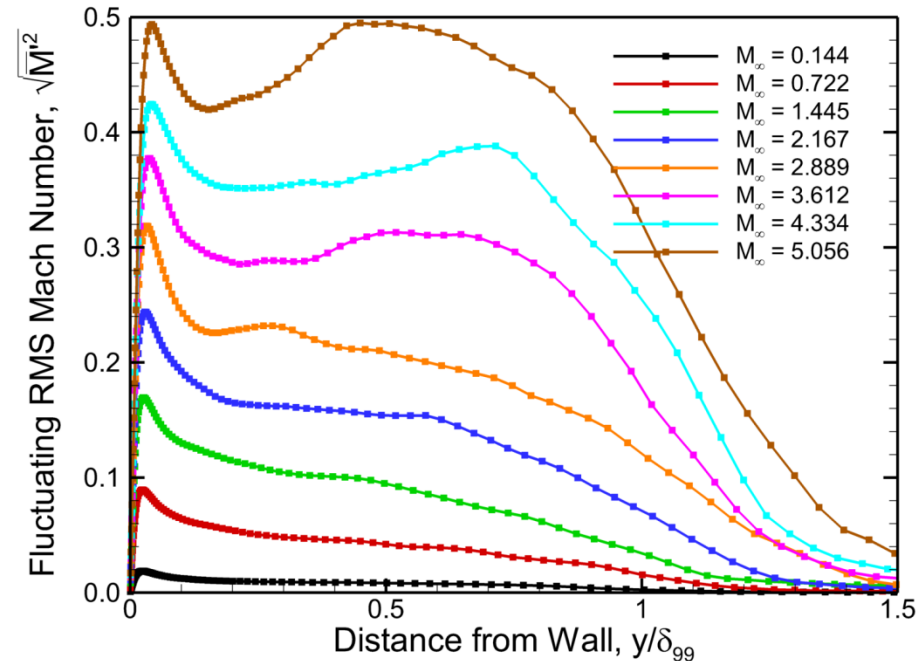


Fluctuating RMS Mach Number Profiles Nominal Reynolds Number Cases on Grid B

SSCD-8



UBR-7

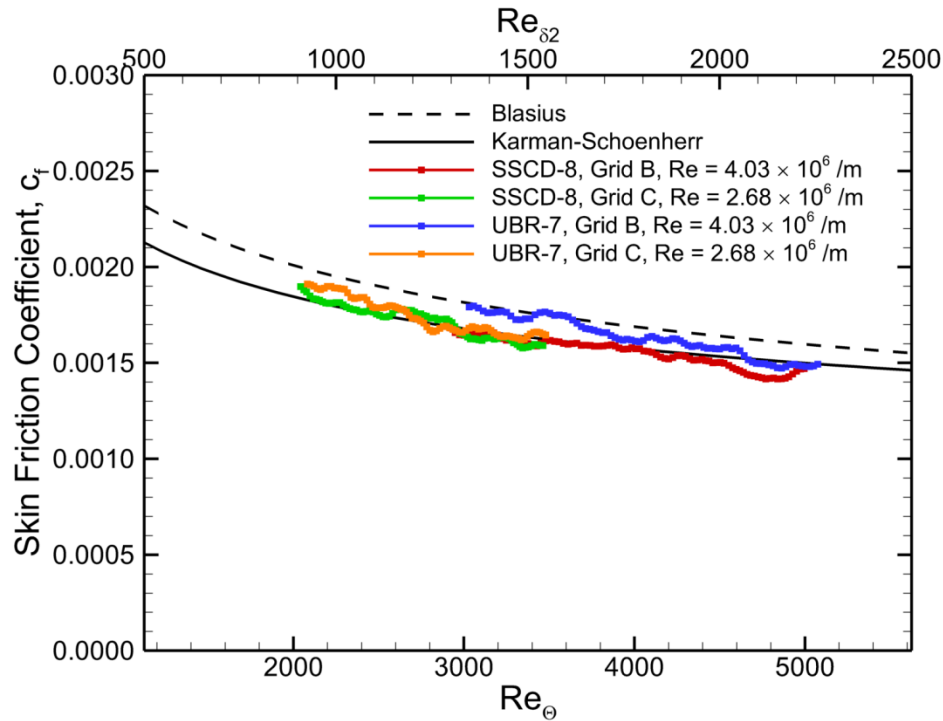


- ◆ Clear increase in fluctuating Mach number with freestream Mach number
- ◆ Some differences in the profiles are evident between the two numerical methods at supersonic conditions. UBR-7 predicts a higher fluctuating Mach number near the wall than SSCD-8 does.
- ◆ The results suggest that fluctuating Mach numbers above 0.34 are problematic for non-dissipative schemes, while dissipative schemes can handle values up to 0.5

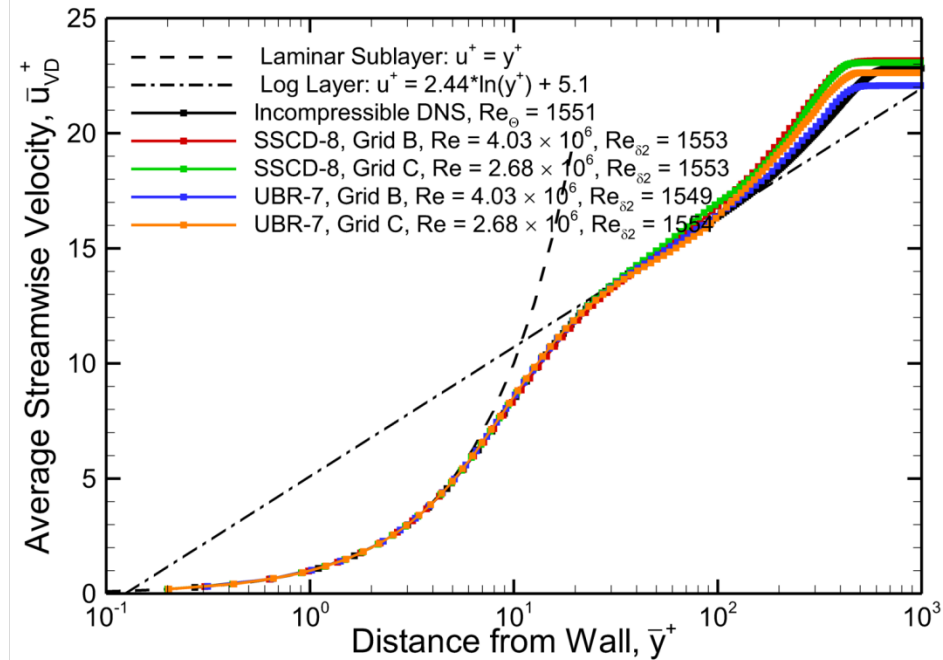


Effect of Grid Resolution on Skin Friction and Velocity Profiles at Mach 3.612

Skin Friction



Mean Velocity Profiles (van Driest-transformed)

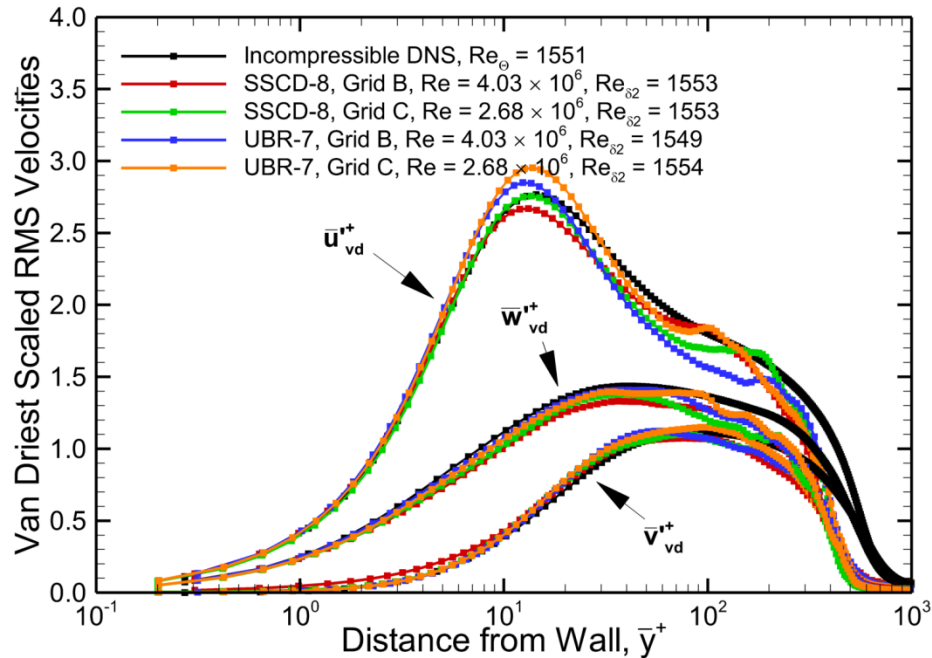


- ◆ Grid B at nominal Reynolds number had $\Delta y_w^+ \approx 0.33$, $\Delta x^+ \approx 16$, $\Delta z^+ \approx 8$
- ◆ Grid C at reduced Reynolds number had $\Delta y_w^+ \approx 0.22$, $\Delta x^+ \approx 8$, $\Delta z^+ \approx 4$
- ◆ Little difference between the two grid resolutions (in wall coordinates) is evident in the results for SSCD-8
- ◆ Higher grid resolution (in wall coordinates) does appear to improve the prediction of skin friction for UBR-7, and also increase the wake strength

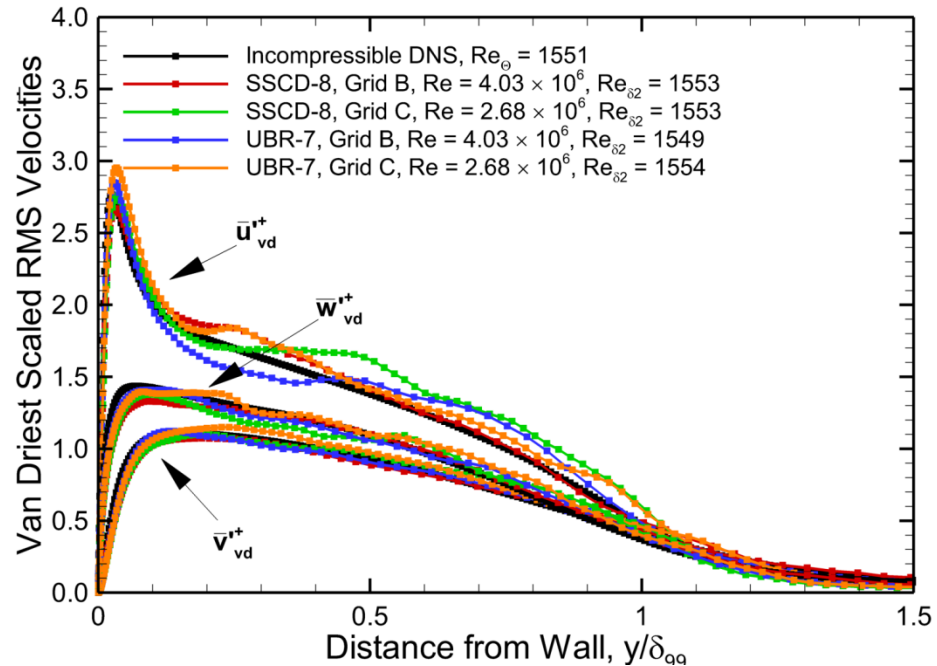


Effect of Grid Resolution on RMS Velocity Components at Mach 3.612

Comparison in Wall Coordinates



Comparison in Outer Coordinates

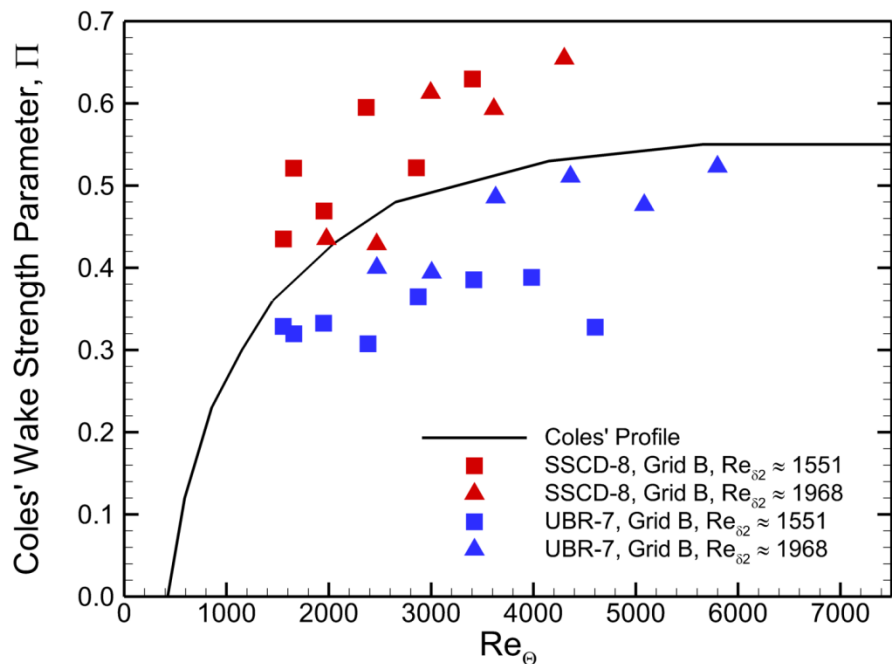


- ◆ Grid B at nominal Reynolds number had $\Delta y_w^+ \approx 0.33$, $\Delta x^+ \approx 16$, $\Delta z^+ \approx 8$
- ◆ Grid C at reduced Reynolds number had $\Delta y_w^+ \approx 0.22$, $\Delta x^+ \approx 8$, $\Delta z^+ \approx 4$
- ◆ UBR-7 at either grid resolution (in wall coordinates) appears to predict higher near-wall peak values of u_{vd}^+ than SSCD-8 does – the difference may narrow at higher resolution
- ◆ Note comparatively lower values of u_{vd}^+ in some of the outer layer (wake region) at the coarser grid resolution – may possibly help explain reduced wake strength

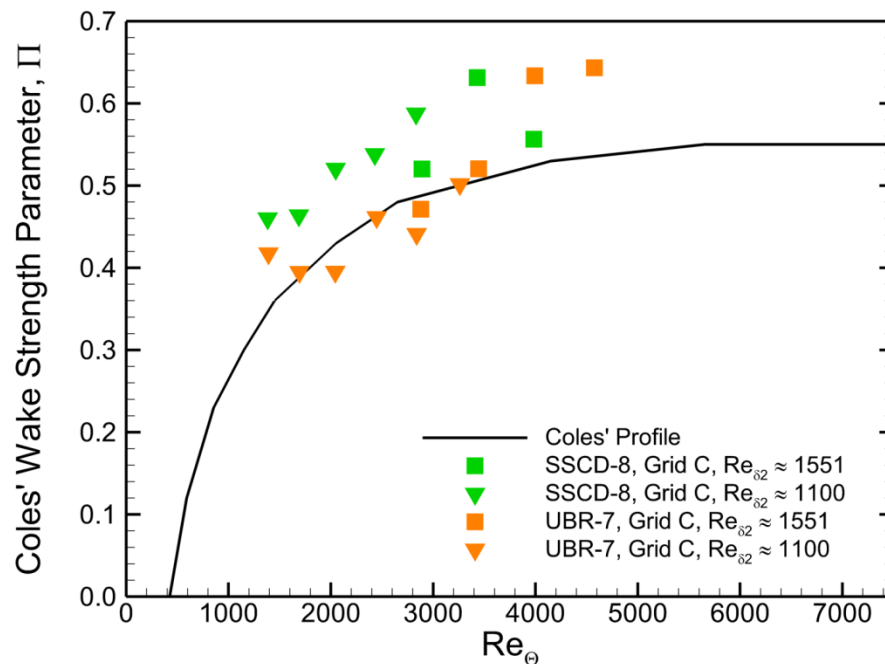


Effect of Grid Resolution on Coles' Wake Strength Parameter

Nominal Reynolds Number Cases
($\Delta y_w^+ \approx 0.33$, $\Delta x^+ \approx 16$, $\Delta z^+ \approx 8$)



Reduced Reynolds Number Cases
($\Delta y_w^+ \approx 0.22$, $\Delta x^+ \approx 8$, $\Delta z^+ \approx 4$)

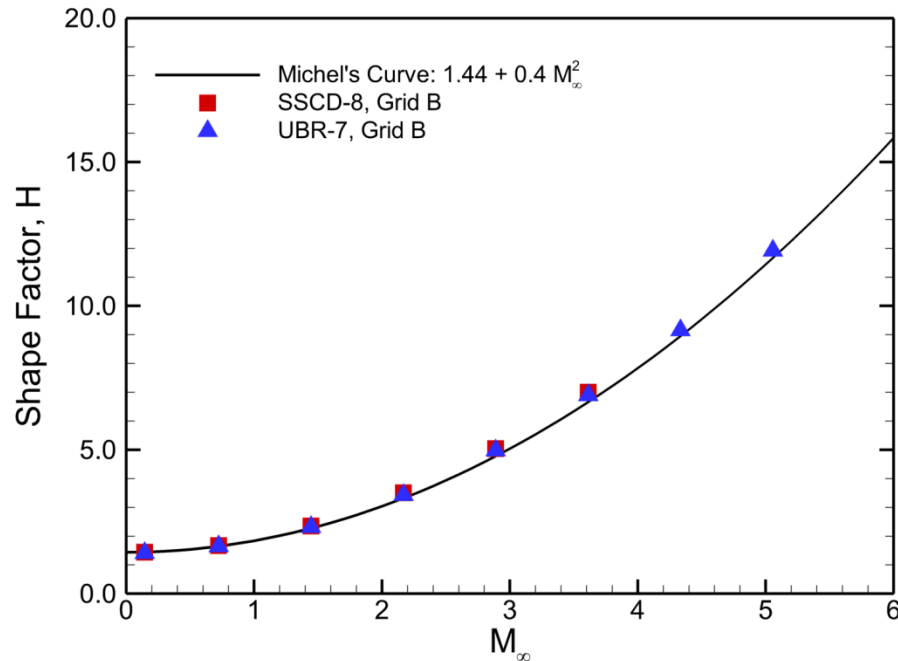


- ◆ The wake strength is the difference between the velocity profile and the log law line at the outer edge of the boundary layer – here the 99% boundary layer thickness was used
- ◆ Coles' Profile for wake strength as a function of Re_θ was compiled from a large set of the available experimental data in the early 1960s
- ◆ The differences between the SSCD-8 and UBR-7 schemes at the coarser grid resolution are evident. The differences narrow considerably at higher grid resolution.

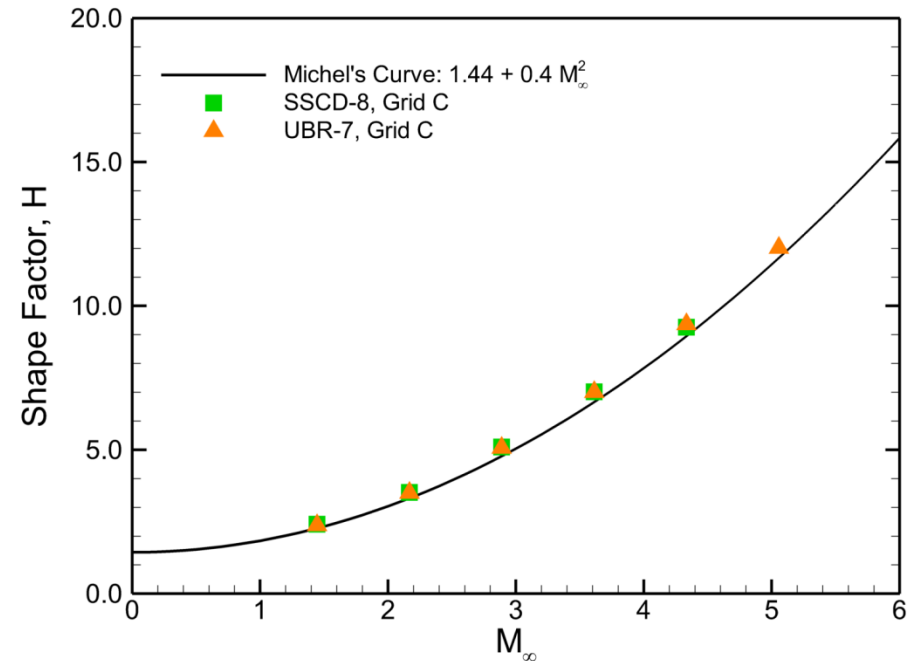


Effect of Grid Resolution on Boundary Layer Shape Factor

Nominal Reynolds Number Cases
($\Delta y_w^+ \approx 0.33$, $\Delta x^+ \approx 16$, $\Delta z^+ \approx 8$)



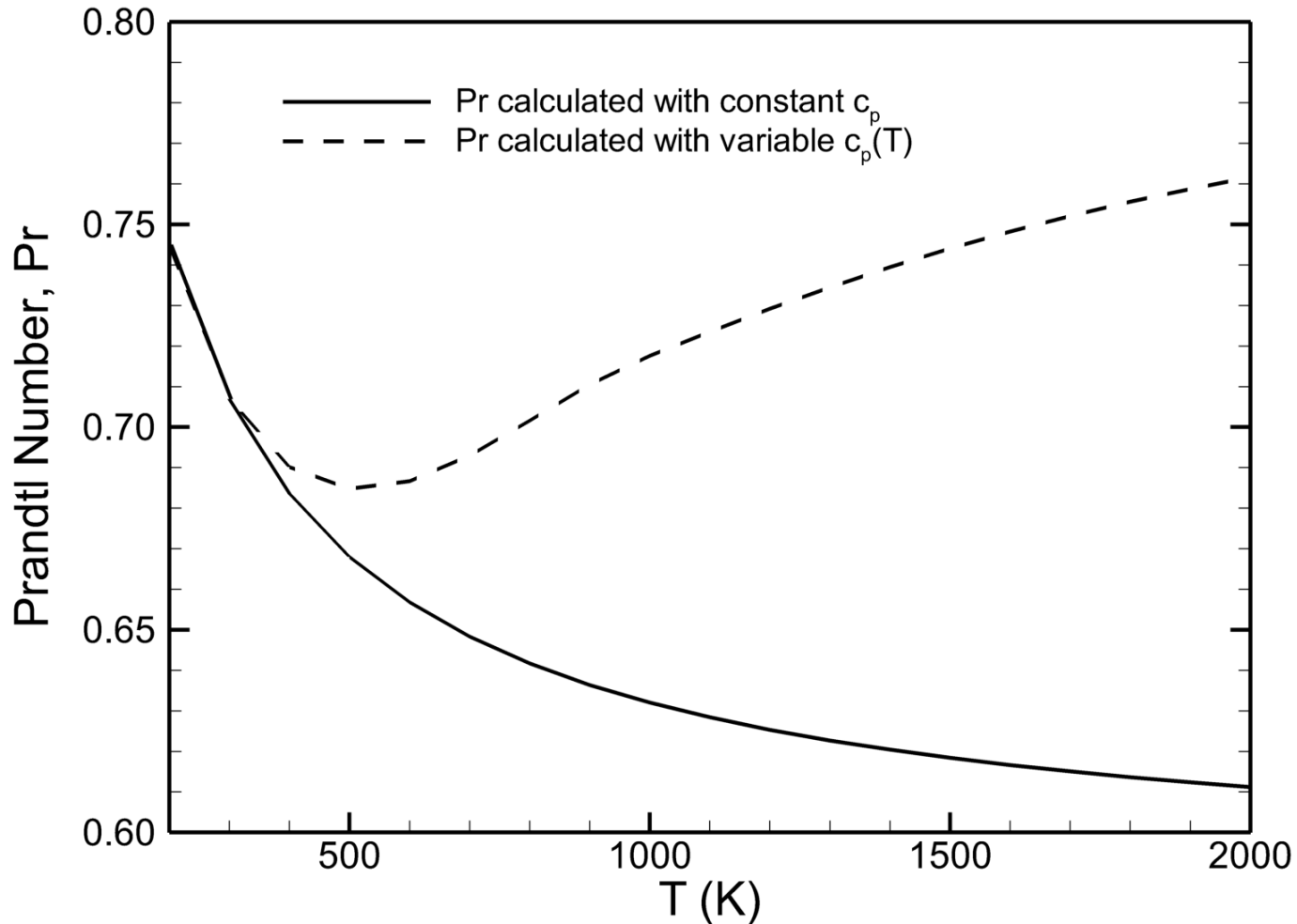
Reduced Reynolds Number Cases
($\Delta y_w^+ \approx 0.22$, $\Delta x^+ \approx 8$, $\Delta z^+ \approx 4$)



- ◆ The boundary layer shape factor, H , is the ratio between the displacement thickness, δ^* , and the momentum thickness, Θ
- ◆ Michel's curve for H (Gatski, 2009) is simple for an adiabatic turbulent boundary layer:
$$H = H_{inc} + 0.4 M_\infty^2$$
- ◆ Both numerical schemes show excellent agreement with Michel's curve. Very little effect from grid resolution is evident.



Effect of Assuming Constant c_p with Sutherland Formulas for μ and λ

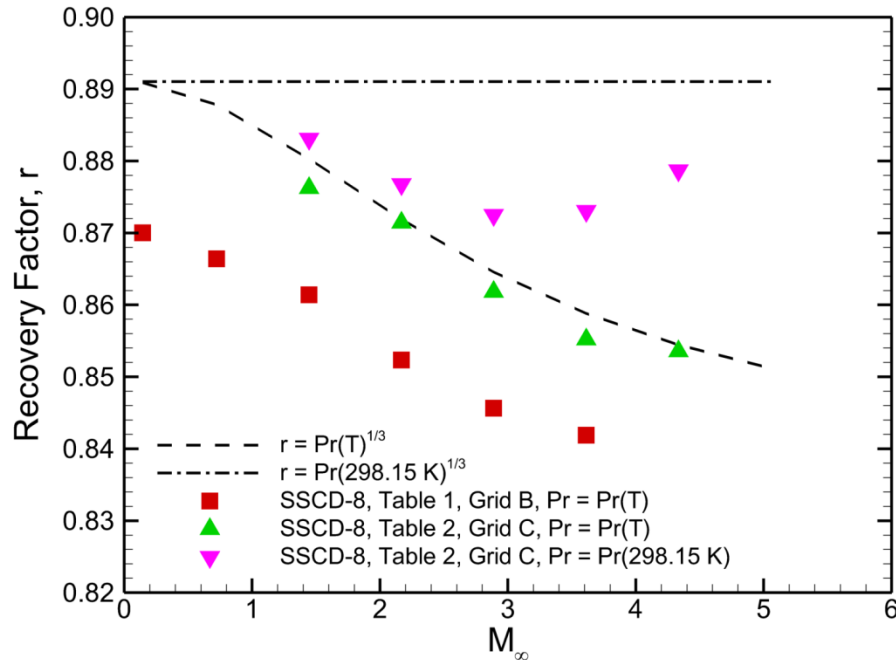


- ◆ This combination of assumptions leads to unrealistically low Prandtl numbers at elevated temperatures – should have used variable c_p , or assumed constant Pr and calculated λ from it ($\lambda = \mu c_p / Pr$)

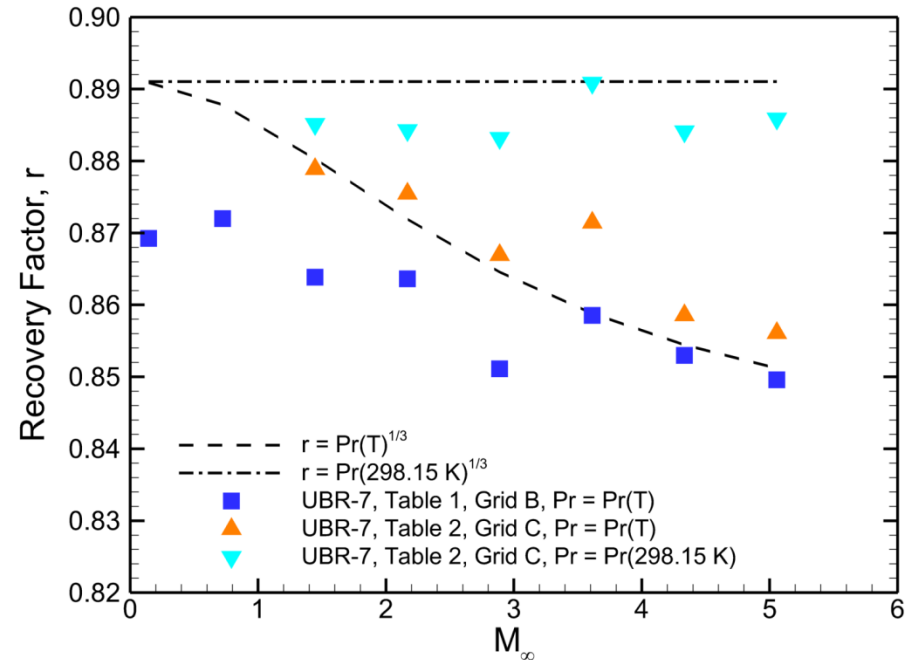


Effect of Grid Resolution, Numerical Scheme and λ on Turbulent Boundary Layer Recovery Factor

SSCD-8



UBR-7



- ◆ The turbulent boundary layer recovery factor is a measure of how much of the total temperature of the flow is actually recovered at the wall in adiabatic flow
- ◆ An additional 11 simulations were run at the highest grid resolution with the assumption of fixed $\text{Pr} = \text{Pr}(298.15 \text{ K})$, and $\lambda = \mu c_p / \text{Pr}$
- ◆ The effect of this assumption on recovery factor is significant
- ◆ Finer wall-normal grid spacing appears to help bring the observed recovery temperature closer to expected values
- ◆ Also note that UBR-7 is typically slightly better here than SSCD-8



Summary

- ◆ **Four non-dissipative skew-symmetric central difference (SSCD-2, SSCD-4, SSCD-6 and SSCD-8) schemes, three upwind-biased Roe (UBR-3, UBR-5 and UBR-7) schemes, and one filtered divergence form central difference (DCD-8-F) scheme were evaluated on a temporally-developing compressible turbulent boundary layer problem.**
- ◆ **The schemes were tested at Mach numbers ranging from effectively incompressible (Mach 0.144) to hypersonic (Mach 5.056). Three different grid sizes were used, and case sets at two different unit Reynolds numbers were run for all of the supersonic cases. The schemes were evaluated in terms of agreement with well-established skin friction and velocity profiles.**
- ◆ **There are clear benefits to higher-order methods for this problem. Among the non-dissipative methods, at the baseline grid resolution in wall coordinates used for much of this work ($\Delta x^+ \approx 16$, $\Delta z^+ \approx 8$), the SSCD-2 scheme clearly became less accurate as the Mach number increased. Further, both SSCD-2 and SSCD-4 became unstable for cases at Mach 3.612 and higher. SSCD-6 and SSCD-8 remained stable at Mach 3.612, and SSCD-8 was stable at Mach 4.334 at the two highest grid resolutions (in wall coordinates) tested. The results suggest that fluctuating Mach numbers above 0.34 become problematic for a non-dissipative scheme, though it appears that fluctuating Mach numbers of 0.43 can be tolerated with higher grid resolution.**



Summary

- ◆ Among the dissipative schemes, UBR-7 offers clear improvements over UBR-3, and to a lesser extent UBR-5, across the entire Mach number range. UBR-3 performed particularly poorly at the lowest Mach number tested, likely due to the relatively higher dissipation characteristics of the Roe solver at low speeds. The DCD-8-F scheme appeared to perform similarly to UBR-7, and possibly slightly better. UBR-7 and DCD-8-F appear to have an excellent combination of accuracy and robustness. The dissipative UBR-7 scheme handled fluctuating Mach numbers up to 0.5 without difficulty.
- ◆ The SSCD-8 and UBR-7 schemes generally performed very similarly on this problem. Some differences between these schemes were noted with respect to turbulence intensities and wake strength at nominal grid resolution in wall coordinates ($\Delta x^+ \approx 8$, $\Delta z^+ \approx 4$). These differences diminished considerably at higher grid resolution ($\Delta x^+ \approx 8$, $\Delta z^+ \approx 4$). The SSCD-8 scheme at both grid resolutions, and the UBR-7 scheme at higher grid resolution, exhibited reasonably good agreement with Coles' fit for wake strength as a function of Re_θ . The SSCD-8 and UBR-7 results also agree well with Michel's formula for boundary layer shape factor as a function of Mach number. Some small differences between the two schemes were noted for the turbulent boundary layer recovery factor. A reduction in Δy_w^+ from ≈ 0.33 to ≈ 0.22 also had a significant effect on the recovery factor.



DNS

Turbulence Modeling Strategies

Directly resolve all scales of turbulent motion. There is no eddy viscosity, and the intrinsic dissipation of the inviscid flux must be \ll laminar viscosity.

LES/ILES

Directly resolve largest scales of turbulent motion, and model the smaller scales using one of two approaches: A) classic LES - a subgrid-scale (SGS) turbulence model, requiring that the intrinsic dissipation of the inviscid flux is \ll SGS eddy viscosity, or B) ILES – where the intrinsic dissipation of a 2nd order accurate inviscid flux approximately mimics the SGS eddy viscosity.

HRANS-LES

Attempts to directly resolve turbulence only in regions with adequate grid resolution, otherwise turbulence is modeled. In LES regions the algorithmic requirements would be consistent with the above description.

RANS

Turbulence is entirely modeled.